

Design, Synthesis, and Biological Evaluation of Potent Dual Agonists of Nuclear and Membrane Bile Acid Receptors

Claudio D'Amore,^{§,||} Francesco Saverio Di Leva,^{†,||} Valentina Sepe,^{‡,||} Barbara Renga,[§] Chiara Del Gaudio,[‡] Maria Valeria D'Auria,[‡] Angela Zampella,^{*,‡} Stefano Fiorucci,[§] and Vittorio Limongelli^{*,‡}

[†]Drug Discovery and Development, Istituto Italiano di Tecnologia, Via Morego, 30, 16163 Genoa, Italy

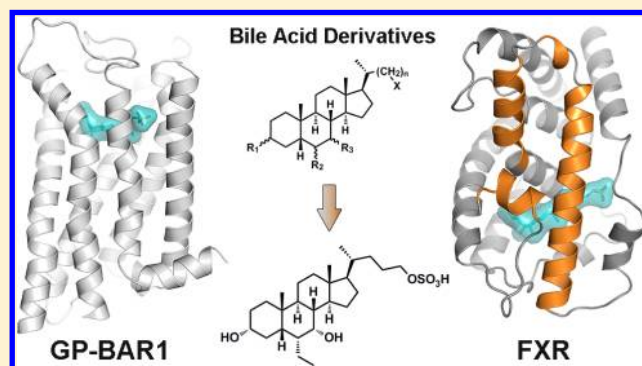
[‡]Dipartimento di Farmacia, Università di Napoli "Federico II", Via D. Montesano, 49, I-80131 Napoli, Italy

[§]Dipartimento di Medicina Clinica e Sperimentale, Nuova Facoltà di Medicina, Università degli Studi di Perugia, Via Gambuli, 1-06132 Perugia, Italy

S Supporting Information

ABSTRACT: Bile acids exert genomic and nongenomic effects by interacting with membrane G-protein-coupled receptors, including the bile acid receptor GP-BAR1, and nuclear receptors, such as the farnesoid X receptor (FXR). These receptors regulate overlapping metabolic functions; thus, GP-BAR1/FXR dual agonists, by enhancing the biological response, represent an innovative strategy for the treatment of enteroendocrine disorders. Here, we report the design, total synthesis, and in vitro/in vivo pharmacological evaluation of a new generation of dual bile acid receptor agonists, with the most potent compound, **19**, showing promising pharmacological profiles. We show that compound **19** activates GP-BAR1, FXR, and FXR regulated genes in the liver, increases the intracellular concentration of cAMP, and stimulates the release

of the potent insulinotropic hormone GLP-1, resulting in a promising drug candidate for the treatment of metabolic disorders. We also elucidate the binding mode of the most potent dual agonists in the two receptors through a series of computations providing the molecular basis for dual GP-BAR1/FXR agonism.



INTRODUCTION

Bile acids (BAs), the end products of cholesterol catabolism, are the main component of bile. Because of their amphipathic nature, bile acids play an essential role in nutrient metabolism and absorption.¹ In the past decade bile acids have been identified as signaling molecules endowed with genomic and nongenomic effects. In 1999 it was demonstrated that primary bile acids act as endogenous ligands for the farnesoid X receptor (FXR), a member of the nuclear receptor superfamily^{2,3} and that chenodeoxycholic acid (CDCA) and its conjugated forms are the most potent endogenous ligands. Acting as an obligatory heterodimer with the retinoid X receptor (RXR), FXR binds to specific responsive elements on promoters of target genes, thus regulating the transcription of enzymes/proteins involved in bile acid synthesis, transport, conjugation, and excretion. Thus, the canonical physiological role for FXR is to function as a bile acid sensor in enterohepatic tissues to maintain bile acid homeostasis. FXR is also involved in regulating critical check points in lipid⁴ and glucose homeostasis.⁵ Furthermore, FXR ligands exert anti-inflammatory⁶ and antifibrotic effects, making this nuclear receptor⁷ an appealing pharmacological target in the treatment of common human diseases ranging from metabolic syndrome to cancer.⁸

In addition to FXR, four nuclear receptors (PXR, CAR, VDR, and LXRs)^{9–11} and G-protein-coupled receptors are known targets for primary or secondary bile acids. The bile acid receptor TGR5 (M-BAR) is a member of the rhodopsin-like superfamily of G-protein-coupled receptor (GPCR)¹² christened as G-protein-coupled bile acid receptor 1, GP-BAR1. GP-BAR1 is highly expressed on the plasma membrane of liver, small intestine, colon, adipose tissue, and skeletal muscle cells as well as in macrophages/monocytes and is activated by secondary bile acids, lithocolic acid (LCA) and tauro-LCA (TLCA).^{13,14} Once activated by secondary bile acids, GP-BAR1 regulates multiple metabolic functions and increases energy expenditure.¹⁵ In enteroendocrine L cells, GP-BAR1 activation stimulates the secretion of glucagon-like peptide (GLP) 1, an insulinotropic factor that enhances insulin release, thus regulating glucose blood levels, gastrointestinal motility, and appetite.¹⁶ In addition, GP-BAR1 has been recently identified as a negative regulator of NF-κB. Indeed, in animal models of liver inflammation, GP-BAR1 activation by 23(S)-methyl-CDCA, a highly selective GP-BAR1 semisynthetic bile acid

Received: October 26, 2013

Published: January 4, 2014

agonist,¹⁷ attenuates the NF- κ B activation induced by LPS through the reduction of I κ B α phosphorylation, thus abrogating NF- κ B translocation into nucleus.¹⁸ In rodent models of colitis, GP-BAR1 expression increases in inflamed tissues while its absence correlates with an increased intestinal permeability and enhanced susceptibility to develop colitis.¹⁹ Moreover, GP-BAR1 was recently demonstrated to be essential in maintaining gastric and intestinal mucosal integrity with a protective effect against gastrointestinal injury caused by nonsteroidal anti-inflammatory drugs.²⁰

Because the two receptors might have overlapping activities, the development of ligands endowed with dual activity toward GP-BAR1 and FXR appears to be an intriguing strategy to target enterohepatic and metabolic disorders.^{21,22} Thus, the 6 α -ethyl-3 α ,7 α -dihydroxy-24-nor-5 β -cholan-23-yl-23-triethylammonium sulfate, also named INT-767 (**1**, Figure 1), a chenodeoxycholic acid derivative acting on both FXR and GP-BAR1, attenuates signs and symptoms of liver injuries in rodent models of metabolic syndrome.^{23–26}

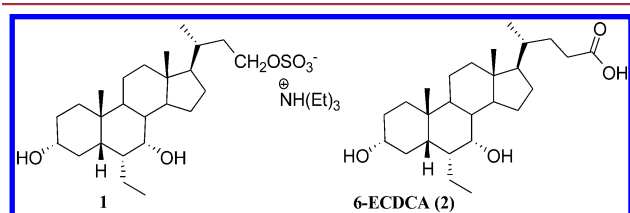


Figure 1. Previously reported dual GP-BAR1/FXR agonists.

Here, using compound **1** as a template for dual GP-BAR1/FXR agonism, we present a new generation of dual bile acid receptor agonists. This strategy resulted in the discovery of compound **19**, the most potent dual agonist of bile acid receptors so far identified, which shows a promising activity for the treatment of diabetes. The binding mode of the most potent GP-BAR1/FXR dual agonists in the two receptors was elucidated through a series of computations using the homology model of GP-BAR1 and the X-ray structure of FXR. Our findings provide the molecular basis for GP-BAR1/FXR dual modulation and are valuable for further investigations on the functional mechanism of bile acid receptors.

RESULTS AND DISCUSSION

Medicinal Chemistry. Even if compound **1** has been investigated as a dual GP-BAR1/FXR agonist,^{24,25} to date, no efficient synthetic procedures have been published. Thus, to have a positive control in biological assays, our research work started with the total synthesis of **1**. From a structural point of view, the most intriguing feature of **1** is the presence of a truncated C23 side chain including a sulfate end-terminus group.

As depicted in the Scheme 1, the synthesis of compound **1** started with the commercially available chenodeoxycholic acid (CDCA, **3**), which was regioselectively oxidized to the C7 hydroxyl group²⁷ and subsequently methylated at C24 carboxyl acid to give methyl ester of 7-ketolithocholic acid (**4**) in a 65% two-step chemical yield. Aldolic addition to a silyl enol ether intermediate²⁸ generated the methyl 3 α -hydroxy-6-ethylidene-7-keto-5 β -cholan-24-oate **5** in a 77% yield. Exocyclic double bond hydrogenation (H₂ on Pd/C) and alkaline hydrolysis of methyl ester functionality on the side chain afforded the useful intermediate acid 3 α -hydroxy-6 α -ethyl-7-keto-5 β -cholan-24-oic

(**7**, quantitative yield). The large coupling constant observed for H-6 proton signal at δ_{H} 2.83 (dd, $J = 13.0, 5.5$ Hz) demonstrates its axial disposition and therefore the α -orientation of the ethyl group at C-6. As previously reported for the total synthesis of solomonsterol B, a C23 sulfate steroid of marine origin endowed with PXR agonistic activity,²⁹ Fisher's esterification with formic acid and acetic anhydride³⁰ generated the performate derivative (**8**) which was subjected to "Beckmann rearrangement" by treatment with sodium nitrite in a trifluoroacetic anhydride/trifluoroacetic acid mixture.³¹

Prolonged alkaline hydrolysis of 23-nitrile derivative **9** afforded 6 α -ethyl-24-nor-7-ketolithocholic acid (**10**) in a 69% three-step chemical yield. Sodium borohydride reduction of the C7-ketone in a mixture of THF/H₂O followed by methanol/*p*-toluenesulfonic acid treatment afforded C23 methyl ester derivative **11** (89% isolated yield in a two-step sequence). ¹H NMR spectrum analysis revealed that the sodium borohydride reduction proceeded in a stereoselective manner, affording the exclusive formation of 3 α ,7 α -dihydroxy-6 α -ethyl-24-nor-5 β -cholan-23-oic acid (see Experimental Section) intermediate, as judged by the shape of H-7 (3.62, br s) which is consistent with an equatorial disposition for this proton and therefore with the axial α -orientation of the hydroxyl group.

Finally, the introduction of the sulfate functional group at C23 was achieved by a three-step sequence including protection of alcoholic functions at C3 and C7, reduction of the methyl ester at C23 with lithium borohydride, and subsequent sulfation with triethylammonium-sulfur trioxide complex at 95 °C (72% three-step chemical yield). Removal of hydroxyl protecting groups through treatment with methanol and a few drops of HCl and purification by reversed-phase solid extraction on a C18 cartridge afforded compound **1** as the triethylammonium salt. HR ESIMS, negative ion mode m/z 471.2795 (calculated 471.2780 for C₂₅H₄₃O₆S), and NMR data (Table S1 in Supporting Information) secured the chemical structure as reported in **1**.

The above synthesis was completed in a total of 15 steps starting from commercially available CDCA (**3**) and was found to proceed with overall yield of 20%.

Derivative **11** was also used as starting material to obtain **13**, a compound with three sulfate groups, respectively, at C3 and C7 on rings A and B and at C23 on the side chain (Scheme 1).

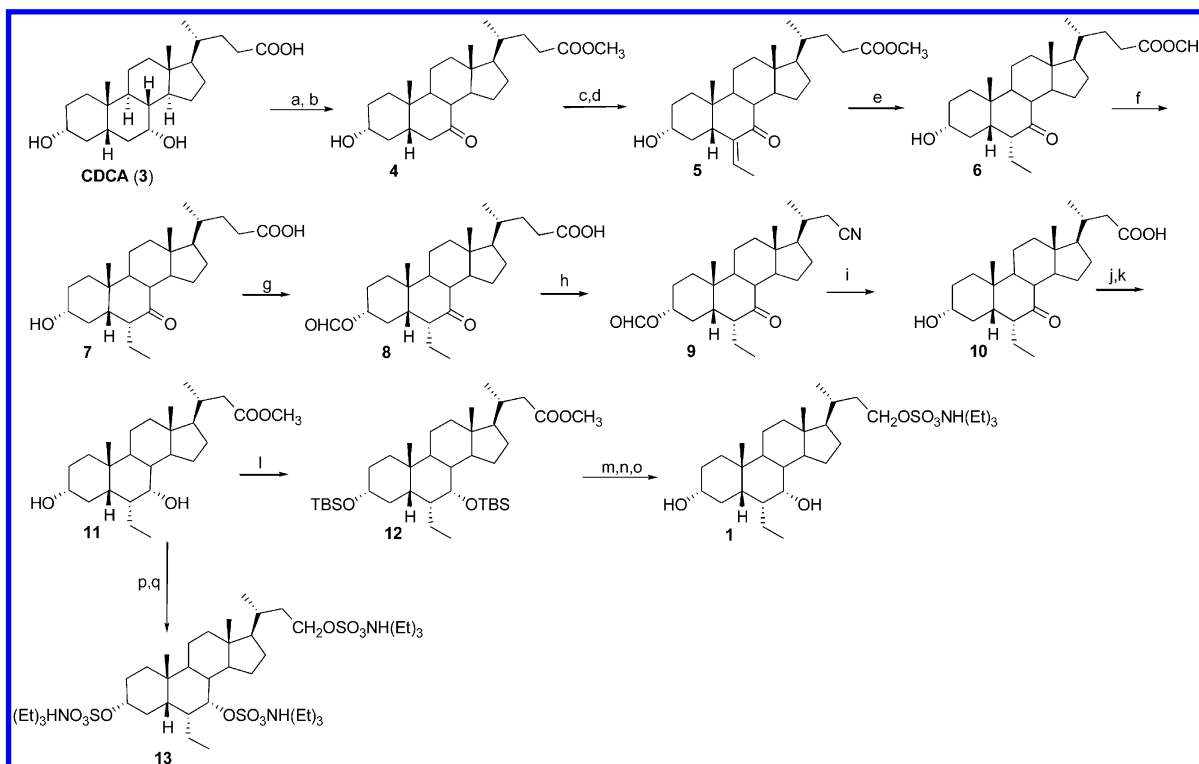
In order to increase the chemical space and investigate the structural requisites for dual GP-BAR1/FXR agonism, we developed a series of bile acid derivatives, modifying bile acid chemical scaffold at different levels: (i) the side chain length (C23 vs C24 and C26), (ii) the presence of sulfate groups on the side chain and on rings A and B of the tetracyclic nucleus, (iii) the configuration at C7, and (iv) the alkylation at C6.

Chenodeoxycholan Sulfate Derivatives. Methyl ester of chenodeoxycholic acid (**14**) was reduced (LiBH₄, MeOH/THF) obtaining the triol **16** in high chemical yield (96%, Scheme 2).

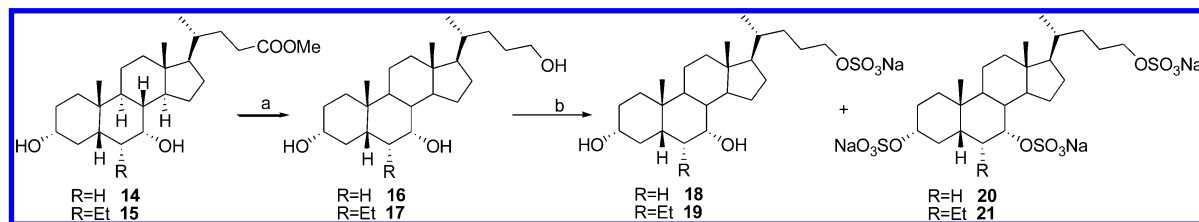
Exhaustive Sulfation (Et₃N·SO₃) and HPLC purification afforded pure chenodeoxycholan sulfate **18** and the corresponding trisulfate derivative **20**.

The same synthetic protocol was applied on the methyl ester of 6-ECDCA (**15**) to produce 6-ethylchenodeoxycholan sulfate **19** and trisulfate derivative **21** (Scheme 2).

tert-Butylsilyl protection on C3 and C7 hydroxyl groups of CDCA methyl ester **14** followed by LiBH₄ reduction afforded alcohol **22** (Scheme 3). Swern oxidation³²/C2 Horner³³ homologation gave the conjugate bis-homo ethyl ester **23**

Scheme 1. Total Synthesis of **1** and Its Trisulfate Derivative **13**^a

^aReagents and conditions: (a) NaBr, TBABr, NaClO 10%, MeOH/AcOH/H₂O/AcOEt 3:1:0.25:6.5; (b) *p*-TsOH, MeOH dry, 65% over two steps; (c) DIPA, *n*-BuLi, TMSCl, TEA dry, THF dry, -78 °C; (d) acetaldehyde, BF₃(OEt)₂, CH₂Cl₂, -60 °C, 77% over two steps; (e) H₂, Pd/C, THF/MeOH 1:1, quantitative yield; (f) NaOH 5% in MeOH/H₂O 1:1 v/v, quantitative yield; (g) HCOOH, HClO₄, 81%; (h) TFA, trifluoroacetic anhydride, NaNO₂; (i) KOH 30% in MeOH/H₂O 1:1 v/v, 86% over two steps; (j) NaBH₄, THF/H₂O 4:1 v/v; (k) *p*-TsOH, MeOH dry, 89% over two steps; (l) 2,6-lutidine, *tert*-butyldimethylsilyl trifluoromethanesulfonate, CH₂Cl₂, 0 °C, 78%; (m) LiBH₄, MeOH dry, THF, 0 °C, 95%; (n) Et₃N·SO₃, DMF, 95 °C; (o) HCl 37%, MeOH, 87% over two steps; (p) LiBH₄, MeOH dry, THF; (q) Et₃N·SO₃, DMF, 95 °C, 72% over two steps.

Scheme 2. Chenodeoxycholan Sulfate Derivatives^a

^aReagents and conditions: (a) LiBH₄, MeOH dry, THF, 0 °C; (b) Et₃N·SO₃, DMF, 95 °C.

whose double bond reduction and silyl deprotection proceeded smoothly affording ethyl ester **24** in 61% yield over six steps. Once again LiBH₄ reduction, sulfation, and HPLC separation gave pure **26** and **27** derivatives (Scheme 3).

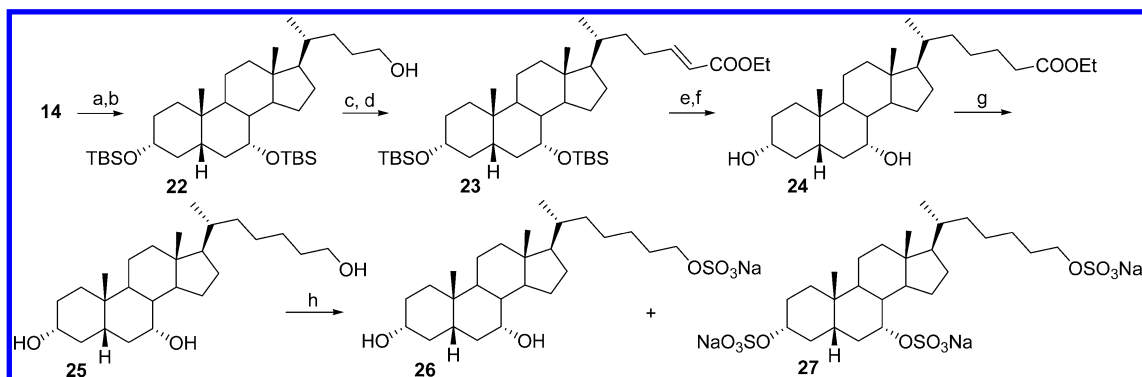
Ursodeoxycholan Sulfate Derivatives. Among BAs, ursodeoxycholic acid (UDCA) is structurally unique, differing in the β -orientation of the hydroxyl group at the C7 position with respect to CDCA. Considering the inactivity of UDCA and its C24 alcohol derivative on FXR,^{2,3,34} structural modification on a 7 β -hydroxylcholanoid scaffold could be instrumental in generating selective GP-BAR1 agonists.

First, silyl protection on UDCA methyl ester **28** followed by reduction, sulfation at C24, and deprotection gave ursodeoxycholan sulfate **30** (55% chemical yield in four steps, Scheme 4, steps a–d). Second, deprotection on derivative **29** and exhaustive sulfation produced a mixture of ursodeoxycholan derivatives (**31**, **32**, **33**) differing in the sulfation pattern and

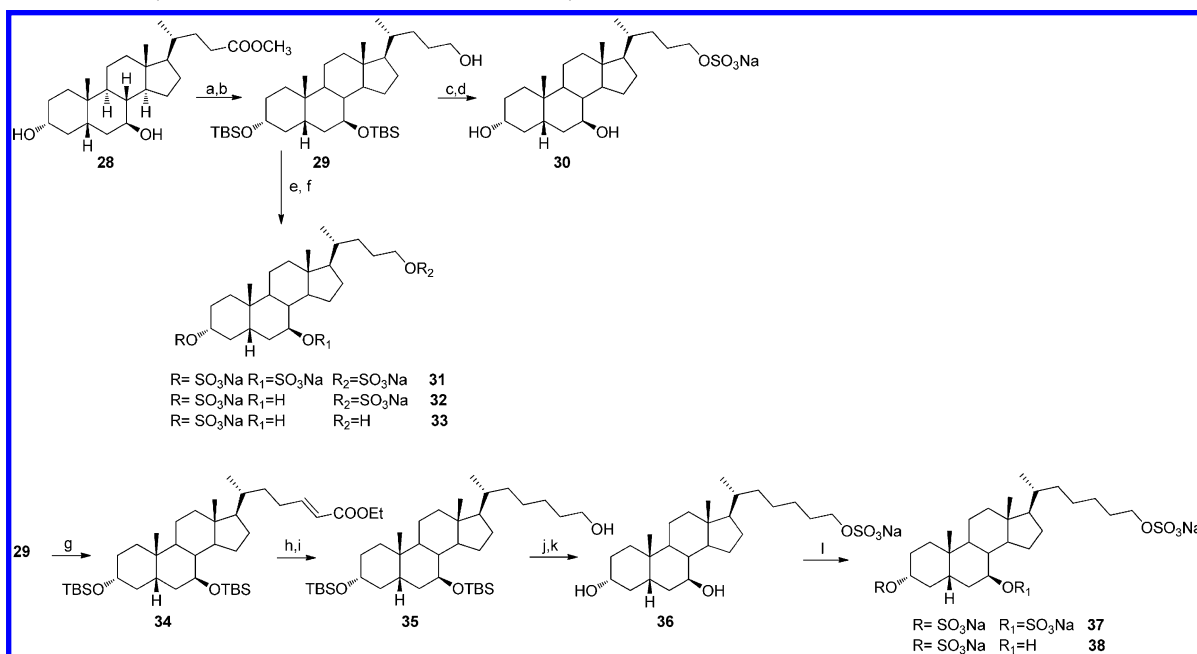
efficiently separated by HPLC (Scheme 4). Bis-homo derivatives (**36**, **37**, **38**) were obtained following the synthetic protocol already described for the corresponding chenodeoxycholan derivatives and depicted in Scheme 4.

Pharmacological Evaluation on the Library. To assess transcriptional activity, all the synthetic derivatives obtained in this study were tested in the luciferase reporter assays on HepG2 cells transfected with human FXR and on HEK-293T cells transfected with human GP-BAR1.

As reported in Figure 2A, in addition to **1** and 6-ECDCA (**2**), already reported as potent FXR agonists, compounds **19** and **26**, 6-ethylchenodeoxycholan sulfate and bis-homochenodeoxycholan sulfate, respectively, were potent inducers of FXR transactivation. Specifically, compound **19** transactivates FXR with the same potency of **1** and **2**. None of the tested compounds turned out to be an FXR antagonist (Figure 2B).

Scheme 3. Bis-homochenodeoxycholan Sulfate Derivatives^a

^aReagents and conditions: (a) 2,6-lutidine, *tert*-butyldimethylsilyl trifluoromethanesulfonate, CH₂Cl₂, 0 °C, 83%; (b) LiBH₄, MeOH dry, THF, 0 °C, quantitative yield; (c) DMSO, oxalyl chloride, TEA dry, CH₂Cl₂, -78 °C; (d) LiOH, TEPA, THF dry, reflux, 91% over two steps; (e) H₂, Pd(OH)₂, degussa type, THF/MeOH 1:1, quantitative yield; (f) HCl 37%, EtOH, 81%; (g) LiBH₄, MeOH dry, THF, 77%; (h) Et₃N·SO₃, DMF, 95 °C.

Scheme 4. Ursodeoxycholan Sulfate and Bis-homoursodeoxycholan Sulfate Derivatives^a

^aReagents and conditions: (a) 2,6-lutidine, *tert*-butyldimethylsilyl trifluoromethanesulfonate, CH₂Cl₂, 0 °C; (b) LiBH₄, MeOH dry, THF, 0 °C, 80% over two steps; (c) Et₃N·SO₃, DMF, 95 °C; (d) HCl 37%, MeOH, 69% over two steps; (e) HCl 37%, MeOH, 96%; (f) Et₃N·SO₃, DMF, 95 °C; (g) DMSO, oxalyl chloride, TEA dry, CH₂Cl₂, -78 °C then LiOH, TEPA, THF dry, reflux, 40% over two steps; (h) H₂, Pd/C, THF/MeOH 1:1, quantitative yield; (i) LiBH₄, MeOH dry, THF, 88%; (j) Et₃N·SO₃, DMF, 95 °C; (k) HCl 37%, MeOH, 75% over two steps; (l) Et₃N·SO₃, DMF, 95 °C.

Similar to what was observed for FXR, results of trans-activations of CREB-responsive elements in HEK-293T transiently transfected with the human membrane bile acid receptor GP-BAR1 revealed that compounds **19** and **26** were potent inducers of cAMP-luciferase reporter gene (Figure 3). Moreover, none of tested compounds were able to induce cAMP-luciferase reporter gene in the absence of GP-BAR1 (Figure S1 in Supporting Information), thus indicating that the above induction is GP-BAR1 mediated. The potency of compound **19** in transactivating CREB responsive element was similar to that of TLCA, the most potent endogenous GP-BAR1 agonist (Figure 3). Forskolin, which increases cAMP in a receptor-independent manner, was used as positive control in these experiments.

Pharmacological Evaluation on Derivative 19, the Most Potent GP-BAR1/FXR Dual Agonist So Far Identified. Because **19** transactivates both FXR and GP-BAR1, we have then investigated the concentration–response curve for this compound. As shown in Figure 4, compound **19** transactivates FXR with an EC₅₀ of ~1 μM (panels A and B) and induces GP-BAR1 activity with an EC₅₀ of ~0.2 μM (panels C and D) and both values were comparable to those previously reported for the reference dual agonist **1**.²⁵ In addition, the efficacy of **19** was 852% and 112% compared to CDCA and TLCA, respectively, thus indicating that compound **19** is a potent GP-BAR1/FXR dual agonist. To further examine the effect of compound **19** on FXR-regulated activities, we have carried out gene expression analysis assessing its activity on three FXR regulated genes, i.e., small heterodimer partner

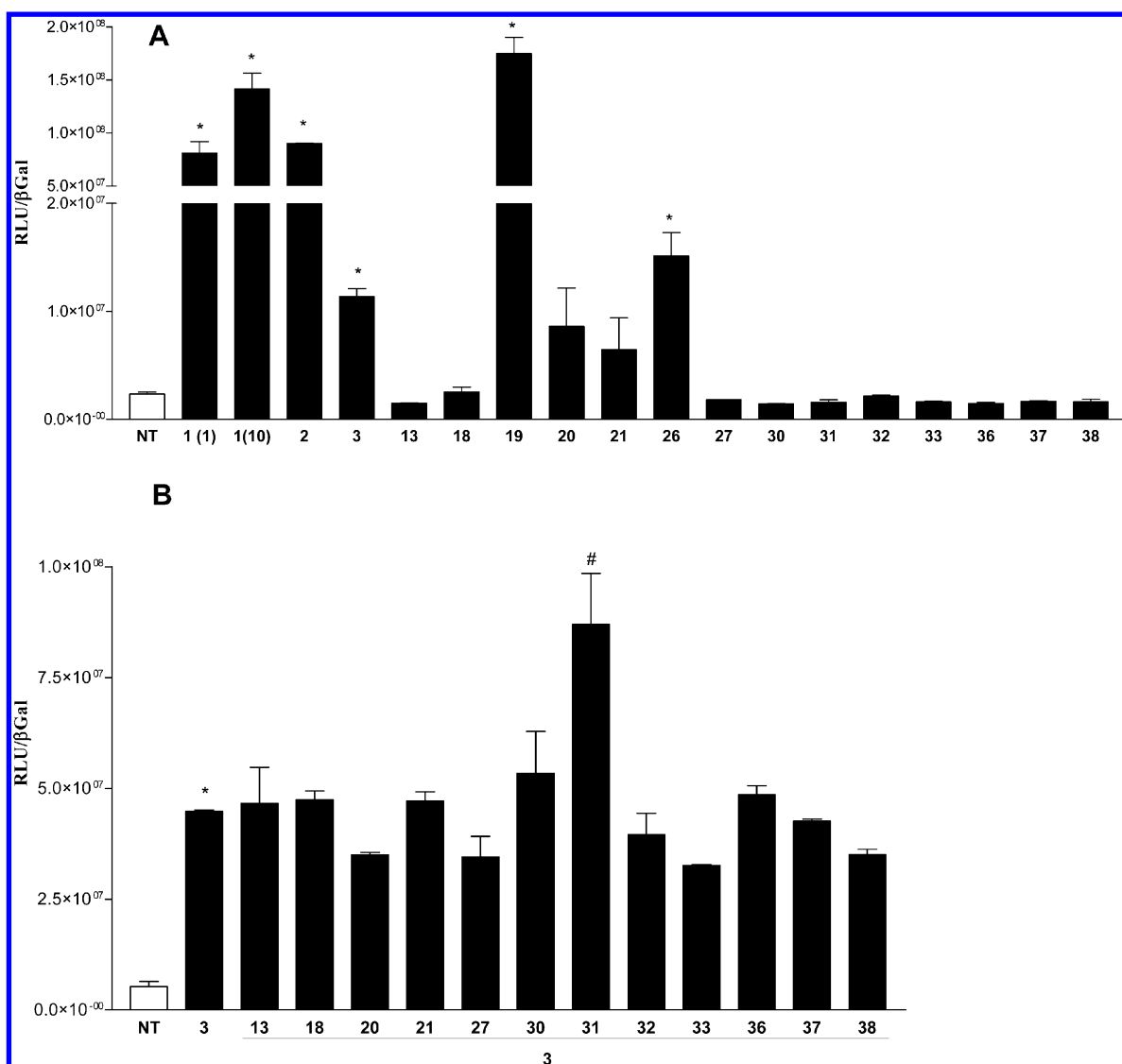


Figure 2. Transactivation assays on FXR. (A) HepG2 cells were transfected with pSG5-FXR, pSG5-RXR, pCMV-βgal, and p(hsp27)TKLUC vectors. Cells were stimulated with 10 μM all tested compounds and with 1 μM compound 1. CDCA (10 μM) was used as a positive control. Results are expressed as the mean ± standard error: (*) $p < 0.05$ vs nontreated cells (NT). (B) HepG2 cells were transfected with pSG5-FXR, pSG5-RXR, pCMV-βgal, and p(hsp27)TKLUC vectors. Cells were stimulated with CDCA, 10 μM, in combination with 50 μM tested compounds. Results are expressed as the mean ± standard error: (*) $p < 0.05$ vs nontreated cells (NT); (#) $p < 0.05$ vs CDCA.

(SHP), organic solute transporter (OST) α , and bile salt export pump (BSEP).

For these purposes, HepG2 cells were used. Results shown in Figure 5, panels A–C, confirmed data reported in Figure 2 and demonstrate that compound **19** is a potent FXR agonist that increases the expression of the three FXR target genes more efficiently than CDCA (**3**), the FXR endogenous ligand, and to a similar extent to 6-ECDCA (**2**), the most potent FXR steroid ligand so far available³⁵ and endowed with promising pharmacological properties.³⁶

We have then examined the effects of **19** on GP-BAR1 on GLUTAg cells. GLUTAg cells³⁷ are an intestinal enteroendocrine cell line, known for their ability to release glucagon-like peptide 1 (GLP-1) in response to GP-BAR1 agonists. This cell line expresses high levels of GP-BAR1 and reacts to receptor binding by a robust generation of cAMP. Therefore, GLUTAg cells are considered a suitable model to evaluate the interactions between GP-BAR1 and its ligands. As illustrated in Figure 5, panel D, compound **19** effectively

increases intracellular concentration of cAMP in GLUTAg cells and is significantly more potent than TLCA, the physiological ligand of GP-BAR1, and 6-ECDCA (**2**). Interestingly, the three compounds caused a robust increase of GLP-1 concentrations in cell supernatants (panel E).

It is worth mentioning that GLP-1 is an appealing pharmacological target in the treatment of diabetes. GLP-1 receptor agonists, like incretins, are currently used in the treatment of type 1 diabetes, although concerns on the safety of these ligands have emerged recently.^{38–42}

Bile acids are potent inducers of GLP-1 release and can therefore hold utility in the treatment of diabetes. The fact that **19** releases GLP-1 from the intestine, without altering its half-life, could result in beneficial effects without increasing the risk of long-acting GLP-1 derivatives.

In addition, the specificity of these interactions in the ability of **19** to modulate FXR was further investigated using FXR^{-/-} cells. As shown in Figure 5, panel F, while compounds **2** and **19** increased BSEP expression in primary hepatocytes isolated

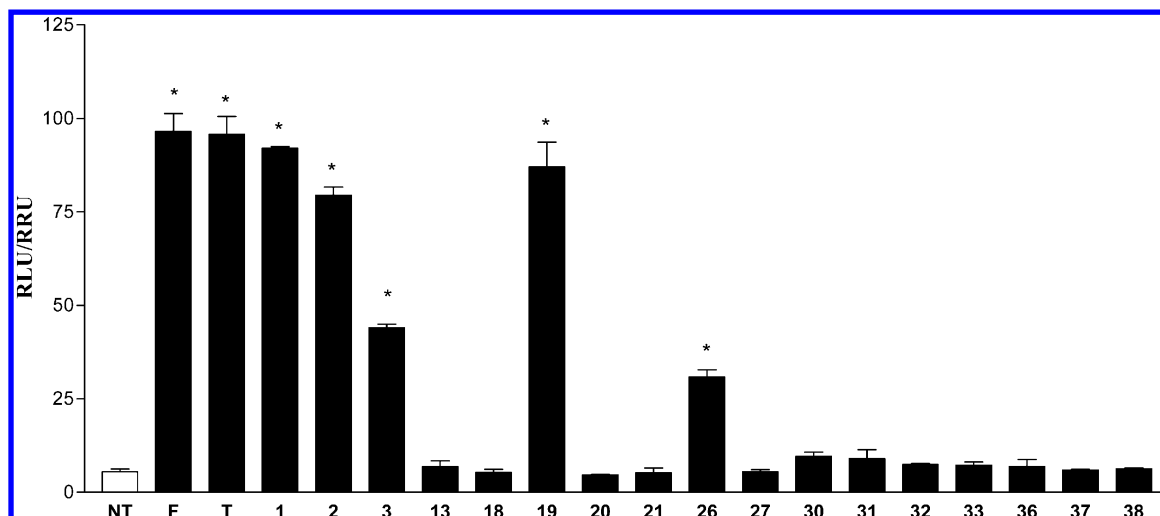


Figure 3. Activation of GP-BAR1. HEK-293T cells were co-transfected with human GP-BAR1 and a reporter gene containing a cAMP responsive element in front of the luciferase gene. At 24 h after transfection, cells were stimulated with 10 μ M compounds 1–3, 13, 18–21, 26–27, 30–33, 36–38. Luciferase activity served as a measure of the rise in intracellular cAMP following activation of GP-BAR1. TLCA (T, 10 μ M) stimulates cAMP production in a GP-BAR1 dependent manner. Forskolin (F, 10 μ M) stimulated cAMP production independently of GP-BAR1. Results are expressed as the mean \pm standard error: (*) $p < 0.05$ vs nontreated cells (NT).

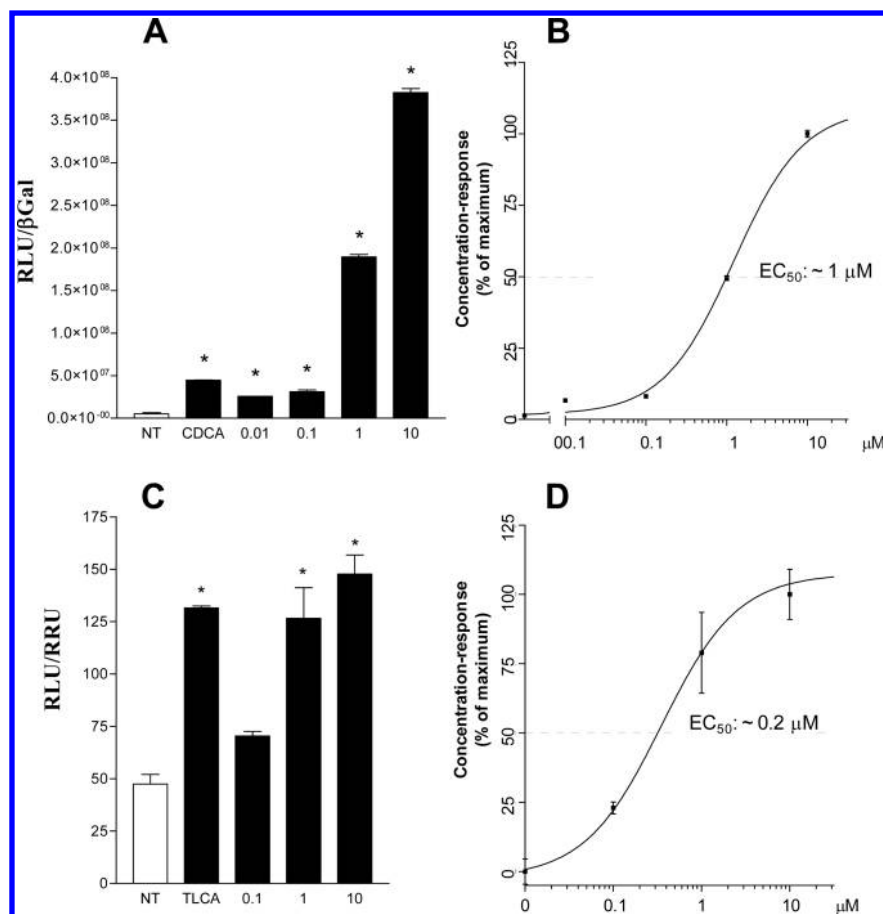


Figure 4. Concentration–response curves for compound 19. (A, B) HepG2 cells were transfected with human FXR and stimulated with increasing concentrations of 19 (0.01, 0.1, 1, and 10 μ M). (C, D) HEK-293T were transfected with human GP-BAR1 and stimulated with increasing concentration of 19 (0.1, 1, and 10 μ M). CDCA (10 μ M) was used as a positive control to evaluate the FXR transactivation. TLCA (10 μ M) was used as a positive control to evaluate the GP-BAR1 activity. Results are expressed as the mean \pm standard error: (*) $p < 0.05$ vs nontreated cells (NT).

from wild type mice, this effect was lost when hepatocytes were prepared from FXR $^{-/-}$ mice.

Computational Studies. To disclose the molecular basis of dual GP-BAR1/FXR agonism, we investigated the binding

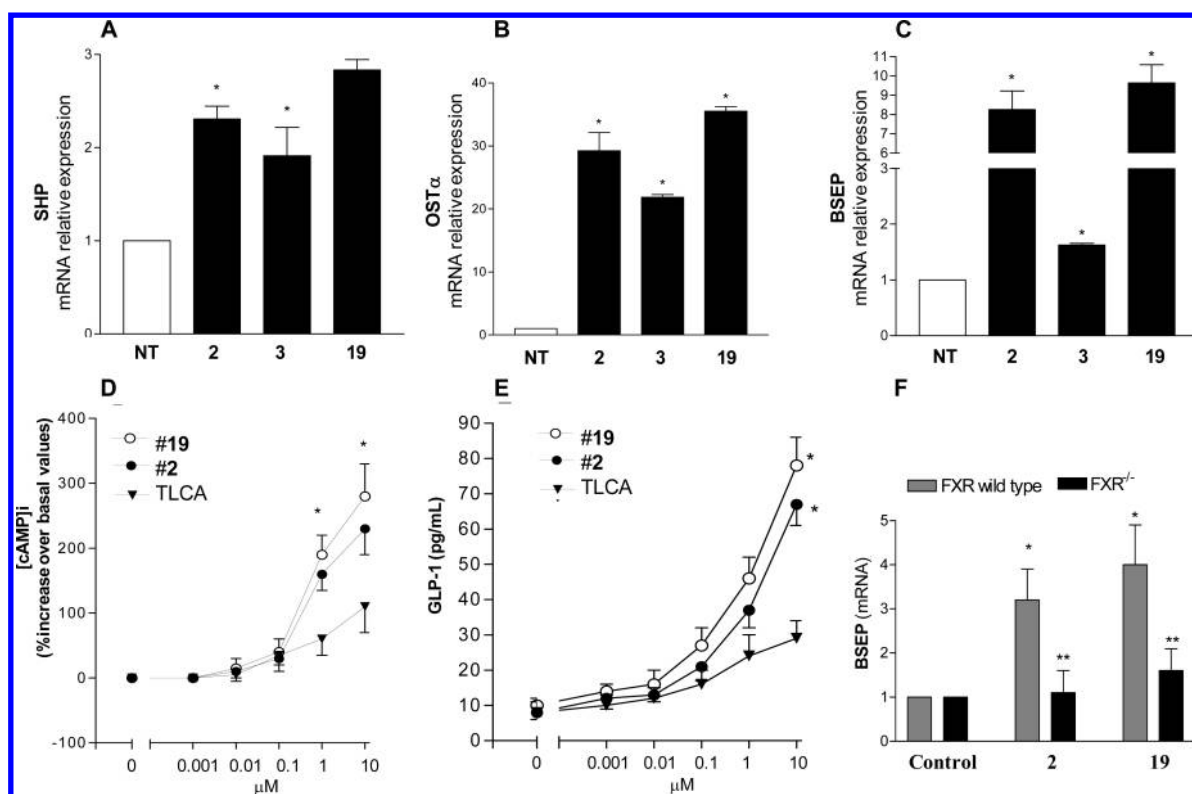


Figure 5. Pharmacological evaluation on derivative **19**, the most potent GP-BAR1/FXR dual agonist so far identified. (A–C) Real-time PCR analysis of mRNA expression of FXR target genes (A) SHP, (B) OST α , and (C) BSEP in HepG2 cells primed with compounds **2**, **3**, and **19**. Values are normalized relative to GAPDH mRNA and are expressed relative to those of nontreated cells (NT), which are arbitrarily set to 1: (*) $p < 0.05$ vs NT. (D, E) Effect of **2** and **19** on intracellular generation of cAMP and GLP-1 release in GLUTAg cells. The data are the mean \pm SE of four to five experiments: (*) $p < 0.05$ vs NT. (F) Compounds **2** and **19** stimulate BSEP expression in wild type hepatocytes but lose their efficacy in hepatocytes obtained from FXR $^{-/-}$ mice. Data are the mean \pm SE of four experiments: (*) $p < 0.05$ vs control and (**) $p > 0.05$ vs wild type cells.

mechanism of the most potent dual agonists, compounds **1** and **19**, to the two receptors, performing a series of computations. While the X-ray structure of FXR has been resolved allowing the discovery of several synthetic and natural ligands,^{21,43} the tridimensional structure of GP-BAR1 has not been determined yet. Therefore, we first decided to build the tridimensional model of this receptor using homology modeling techniques (Figure 6A and Figure 6B). As template structure, we choose the agonist conformation of the adenosine A_{2A} receptor (PDB code 2ydo),⁴⁴ which shows one of the highest sequence identity and similarity values, 20% and 55%, respectively (see Supporting Information for details and Figure S2). This model, together with the crystal structure of FXR, was used in the subsequent docking study to disclose the binding mode of compounds **1** and **19** in the two receptors and then to define the structural requirements for dual GP-BAR1/FXR agonism.

Binding Mode of 1 in GP-BAR1 and FXR. To take into account the receptor flexibility, 10 different GP-BAR1 conformations, obtained from the MD simulation on the apo form of the receptor, were considered for the docking calculations of compound **1** (see Supporting Information). The AutoDock4.2 docking program⁴⁵ found similar binding results in the different receptor conformations, with the most populated clusters showing the ligand occupying the region underneath the extracellular loop II. However, most of the docking solutions were not fully in agreement with the requisites necessary for the binding of bile acid derivatives to GP-BAR1 reported in literature.⁴⁶ These include (i) the interaction of the 3 α and/or 7 α hydroxyl groups with a

negatively charged region in the binding site, (ii) the insertion of the side chain at C17 position into a rather large and polar cavity, (iii) the insertion of the alkyl substituent at C6 position into an ancillary hydrophobic pocket. The inaccuracy of docking calculations was probably due to the conformations of the side chains of the binding site residues, which in the apo form are different with respect to the agonist-bound state. To overcome this limitation, we had to step up the computational strategy and take into account the full receptor flexibility. In such a way, even difficult ligand/protein binding mechanisms can be elucidated.^{47–49} In this case, molecular dynamics (MD) simulations on the **1**/GP-BAR1 complex embedded in a POPC bilayer surrounded by explicit water were carried out. In this calculation, the docking pose that fulfilled most of the aforementioned structural requirements for the binding was selected as starting conformation. Then we performed steered MD simulations to refine the ligand binding conformation optimizing the distance and orientation of the ligand–protein interactions. The obtained complex was equilibrated and underwent an over-100 ns MD simulation during which the whole system was fully flexible. The ligand binding conformation, depicted in Figure 6C, was stable throughout the whole simulation, as shown by the low rmsd value reported in Figure 6D, with all the ligand–protein interactions conserved. In particular, the ligand 3 α -hydroxyl group H-bonds with Glu169 and interacts via a water molecule with Tyr240 side chain, while the 7 α -hydroxyl group is involved in a H-bond with Asn93 and water-mediated interactions with Tyr89 and Glu169. On the other side, the sulfate side chain points toward

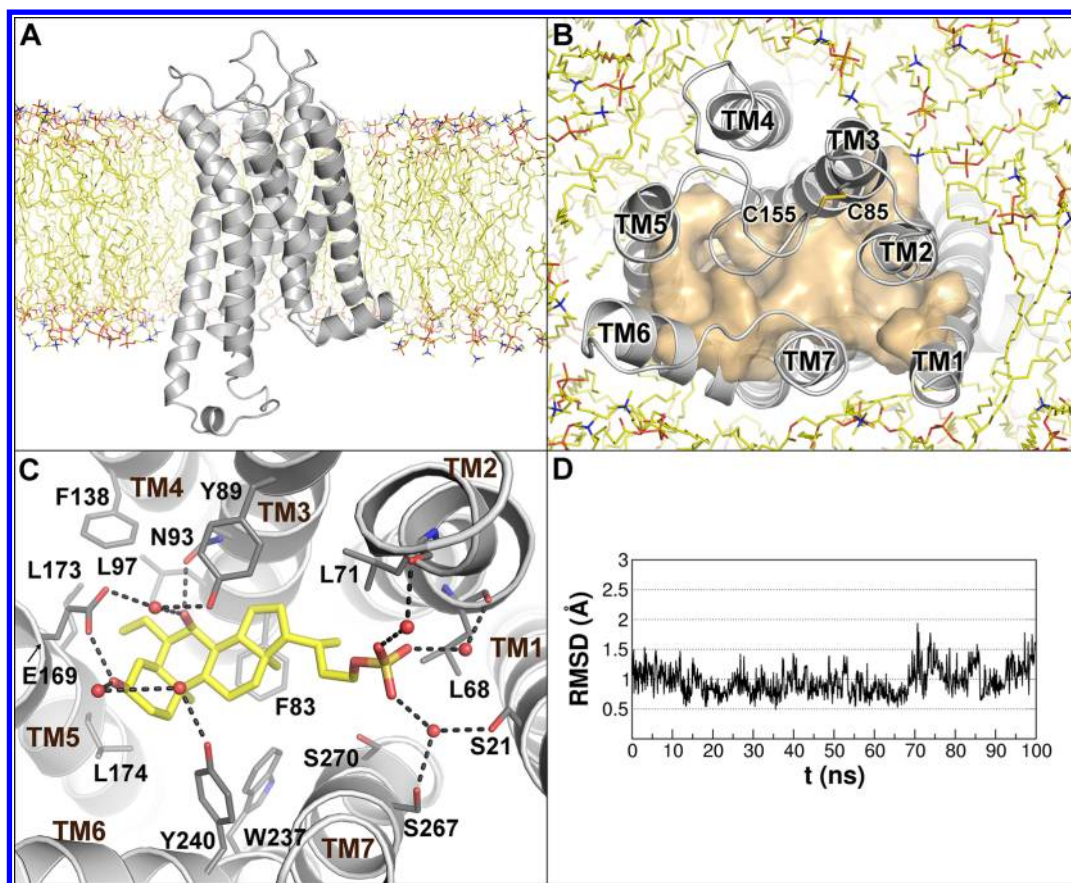


Figure 6. Tridimensional model of GP-BAR1 and binding mode of **1**. Side (A) and top (B) views of the tridimensional model of the GP-BAR1 receptor embedded in the POPC bilayer. The receptor is shown as gray cartoons. Lipids are depicted as yellow sticks. The ligand binding cavity (B) is shown as transparent orange surface. Residue numbers were assigned according to the amino acid sequence of hGP-BAR1. (C) Binding mode of **1** obtained through over 100 ns long MD simulation. The ligand and interacting residues are represented as yellow and gray licorice, respectively, while the GP-BAR1 receptor is shown as gray cartoons. Water molecules are displayed as spheres, while all the hydrogens are omitted for clarity reasons. (D) The rmsd plot of the ligand heavy atoms during the production MD run. Prior to the rmsd calculations, trajectory frames were aligned using the coordinates of the $C\alpha$ carbons of the transmembrane helices.

helices I, II, and VII where the ligand can establish water-mediated interactions with the side chains of Ser21 and Ser267 and with the backbone CO groups of Leu68 and Leu71.

The steroidal scaffold engages several hydrophobic interactions with Leu71, Phe83, Leu174, and Trp237, further stabilizing the ligand binding mode.

The 6-ethyl group of **1** deepens in a hydrophobic pocket formed by residues Leu97, Phe138, Leu173, and Leu174. The peculiar shape and lipophilicity of this pocket suggest the importance of having short and hydrophobic chains at the C-6 position on the steroidal scaffold to achieve optimal GP-BAR1 agonist activity. The proposed ligand binding mode is in full agreement with the structural features required for GP-BAR1 binding⁴⁶ and is further substantiated by recent mutagenesis data,⁵⁰ reporting a decrease of the binding affinity for ligands similar to **1** in Asn93Ala, Glu169Ala, and Tyr240Ala mutant forms of GP-BAR1. These findings and the stability of the ligand–protein interactions along the MD simulation support the reliability of our receptor model and the proposed binding mode.

A movie showing the stability of the ligand binding mode during the 100 ns MD simulation can be found as Supporting Information.

To elucidate the binding mode of **1** to FXR ligand binding domain (FXR-LBD), molecular docking calculations were

performed using the crystal structure of the FXR-LBD from *Rattus norvegicus* (rFXR) in complex with 6-ethylchenodeoxycholic acid (6-ECDCA, **2**), a semisynthetic GP-BAR1/FXR dual agonist bile acid derivative with a FXR binding affinity that is significantly greater than the endogenous ligand CDCA,³⁵ and the GRIP-1 coactivator peptide NID-3 (PDB code 1osv).⁵¹ rFXR-LBD shares the 95% of homology with that of the human FXR-LBD (hFXR-LBD), with all of the residues in the ligand binding pocket conserved among the two species. For docking studies we again used the AutoDock4.2 software (AD4.2), which has been successfully used in our previous computational studies on NRs.⁵² The best scored and most occurring ligand docking conformation shows **1** bound to the cavity formed by helices H3, H5, H7, H11, and H12 (Figure 7).

Here, the steroidal scaffold establishes favorable hydrophobic interactions with the side chains of Met262, Met287, Ala288, and Trp466, while the sulfate group salt-bridges with the Arg328 guanidinium group. In addition, the 3 α -OH H-bonds with the side chains of Tyr358 and the protonated His444, while the 7 α -OH H-bonds with the Ser329 and Tyr366 hydroxyl groups. The latter residue together with Tyr358, Ile359, and Phe363 also engages hydrophobic contacts with the 6-ethyl substituent, further stabilizing the binding pose. Overall, the binding mode is very similar to that experimentally found for 6-ECDCA.⁵¹ In fact, like 6-ECDCA, **1** interacts through its

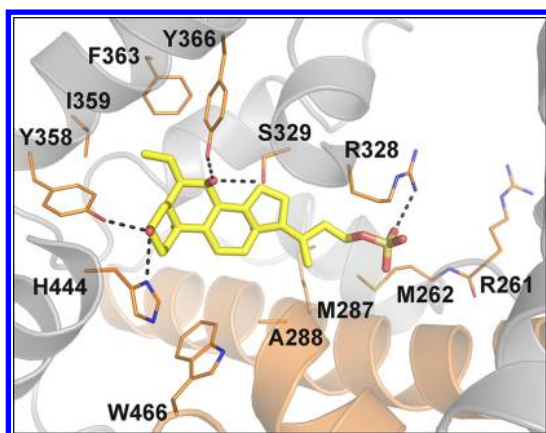


Figure 7. Binding mode of **1** in FXR. The ligand is depicted as yellow sticks, respectively. FXR is shown as orange (helices H3, H4, and H12) and gray cartoons. Amino acids involved in ligand binding are shown as orange sticks. Hydrogens are omitted for clarity.

3 α -OH group with Tyr358 on helix H11 and with His444 on helix H12, contributing to stabilization of the cation– π interaction between His444 and Trp466 in the AF-2 domain. This interaction favors helices H3, H4, H11, and particularly H12 to adopt a conformation competent for the binding of coactivator peptides, thus inducing the transcription of target genes. Moreover, similar to the carboxylate group of 6-ECDCa, the sulfate moiety of **1** salt-bridges with the Arg328 side chain. This interaction, as well as the aforementioned cation– π between Tyr358 on H11 and His444 on H12, is important for the activation of FXR by bile acid derivatives.⁵¹

Insight on Structural Requisites for Dual GP-BAR1/FXR Agonism. Docking calculations in the GP-BAR1 and FXR binding sites were performed on the most potent dual agonist of the series, compound **19**. For these calculations the GP-BAR1 conformation obtained from the MD simulation on the **1**/GP-BAR1 complex was used. The quality of this structure was assessed using the MolProbity server (<http://molprobity.biochem.duke.edu>) showing 100% of all residues in allowed conformational regions according to the Ramachandran analysis (Figure S3). For this ligand, docking calculations found, among the best scored solutions, a binding mode very similar to those of **1** in the two receptors (Figure 8). Using these results, we were able to define the structural requisites to have mutually active ligands on the two targets. In fact,

although GP-BAR1 and FXR are structurally very different, the active ligands show common structural features. In particular, side chain elongation led to derivative **19**, which is the most potent compound of the series toward both targets. Compound **19** occupies the GP-BAR1 binding site similarly to **1** (Figure 8A). However, different from **1**, the **19** side chain can engage direct (i.e., not water-mediated) H-bonds with the Ser21, Ser267, and Ser270 residues on helices TM1 and TM7, thus explaining the improved agonist profile of **19** in comparison with **1**.

In the FXR site, the sulfate group of **19** engages a salt-bridge interaction with the side chain of Arg328 in a way similar to **1**. At variance with **1**, compound **19** is also able to H-bond with the backbone NH of Met262 in the loop connecting helices H1 and H2, and the sulfate group is close enough to interact with the Arg261 side chain (Figure 8B). The latter interactions further stabilize the binding mode of this ligand, thus explaining the higher activity of **19** if compared with that of **1**. It is interesting to note that docking calculations show that even shorter side chains, as in the case of **2**, are allowed, since the ligand is able to interact with at least one serine residue in GP-BAR1 (Figure S5A in Supporting Information) and with Arg328 in FXR (Figure S5B in Supporting Information). Furthermore, the presence of the sulfate group on the side chain is preferable to the carboxylate, since these groups are placed in solvent accessible regions in both receptors, where the sulfate is able to establish a larger number of interactions with water molecules and surrounding residues. Finally, docking studies would suggest that a negatively charged group is not strictly necessary; however, a polar group, able to form H-bond interactions, is desirable to activate GP-BAR1. On the other hand, a negatively charged group is required to activate FXR interacting with either Arg328 or Arg261 or both residues in the FXR-LBD.

On the other side, the presence of the ethyl group and hydroxyl group at C6 and C7, respectively, and their configuration are important for the dual activity. In fact, the most potent agonists of the series, compounds **1**, **2**, and **19**, have both these groups in the α configuration. In GP-BAR1, while the ligand 7 α -OH group H-bonds with Asn93, the 6 α -ethyl deepens into a hydrophobic pocket formed by Leu97, Phe138, and Leu173. These nonpolar interactions are important to stabilize the ligand binding conformation. In fact, compounds that do not present the 6 α -ethyl group show a lower activity (e.g., compare **2** vs **3** and **18** vs **19**). In FXR,

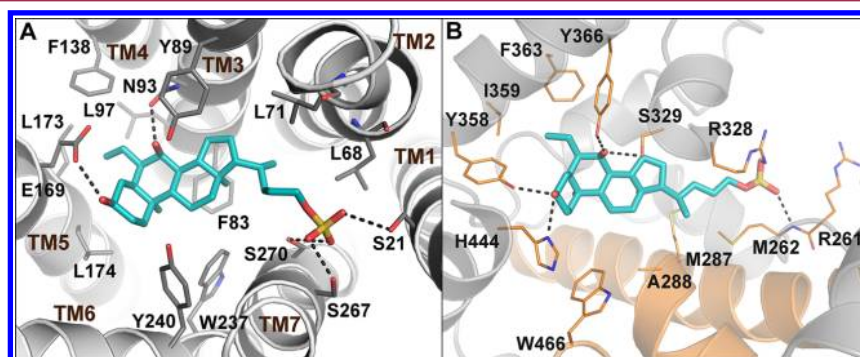


Figure 8. Binding mode of **19** in GP-BAR1 and in FXR. (A) Conformation obtained from MD simulations on the **1**/GP-BAR1 complex. (B) Conformation obtained from MD simulations within rFXR-LBD (PDB code 1osv). Compound **19** is represented as cyan sticks. The receptors are shown as gray and orange (helices H3, H4, and H12 in FXR) cartoons. Amino acids involved in ligand binding are depicted as gray (in GP-BAR1) and orange (in FXR) sticks. Hydrogens are omitted for clarity.

similar to what was observed for **1**, the 7 α -OH of **2** and **19** H-bonds with the Ser329 and Tyr366 hydroxyl groups while the 6 α -ethyl substituent inserts into the hydrophobic pocket formed by Tyr358, Ile359, Phe363, and Tyr366. As for GP-BAR1, also in FXR the absence of the 6 α -ethyl group leads to less active compounds (compare **2** vs **3** and **18** vs **19**). It is interesting to note that despite the lack of the 6 α -ethyl group, **26** is still able to activate, albeit to a minor extent than the more potent derivatives **1**, **2**, and **19**, both GP-BAR1 and FXR in transactivation assays (Figure 2A and 3). This can be ascribed to the presence of a longer side chain allowing the ligand to tightly interact with the serine residues on helices TM1 and TM7 in GP-BAR1 and with the Arg261 and Arg328 side chains in FXR.

Furthermore, as shown in Figures 2 and 3, all ursodeoxycholan sulfate (**30–33**) and bis-homoursodeoxycholan sulfate derivatives (**36–38**) were inactive toward both receptors. These findings demonstrate that despite the presence of one or more sulfate groups on the UDCA scaffold, the configuration at C7 once more plays a fundamental role to properly accommodate the molecules in the binding sites of the receptors. In fact, inverted configuration does not allow the 7-OH group to interact with Tyr89 and Asn93 on TM3 in GP-BAR1 and with Ser329 and Tyr366 in the FXR-LBD. The loss of these interactions, together with the lack of the 6 α -ethyl substituent on the UDCA scaffold, can explain the inability of these derivatives to activate either GP-BAR1 or FXR in transactivation assays.

Finally, independent from the side chain length and the alkylation at C6, the introduction of additional sulfate groups on rings A and B produces a loss in the activity of cholane derivatives toward both receptors (compare **1** vs **13**, **26** vs **27**, and **19** vs **21** in Figures 2 and 3). This effect might be addressed to the bulkiness and the highly negative charge of these groups, which can play a negative role in the ligand/receptor binding process in both GP-BAR1 and FXR.

CONCLUSIONS

In the present study, bile acid derivatives have been developed leading to the identification of compound **19**, which is the most potent GP-BAR1/FXR dual agonist reported so far. In particular, **19** transactivates FXR and increases the expression of FXR-regulated genes in the liver. On the other hand, **19** increases CREB transactivation, a measure of its GP-BAR1 agonism in HEK-293T cells transfected with the membrane receptor. Furthermore, the activity of **19** on GP-BAR1 was also confirmed on cell lines known to respond to GP-BAR1 ligands, GLUTAg cells.⁵³ In vivo and in vitro studies have shown that **19** increases the intracellular concentration of cAMP and stimulates the release of the potent insulinotropic hormone GLP-1,³⁷ thus representing a promising lead for the treatment of insulin-dependent conditions including diabetes. Furthermore, the binding mode of the most potent dual agonist to GP-BAR1 and FXR was elucidated through a series of computational studies. These simulations also provided the molecular bases to achieve potent GP-BAR1/FXR dual agonism. Despite its potent GP-BAR1 activity, **19** maintains the ability to stimulate FXR and FXR-target genes including BSEP. This remains a potential drawback because FXR activation worsens liver injury in rodent model of cholestasis, and therefore, the use of dual GP-BAR1/FXR agonist might have similar side effects of selective FXR ligands.⁵⁴

In conclusion, this study is relevant for further investigations on the functional mechanism of these two receptors and for the design of novel dual GP-BAR1/FXR agonists, providing new opportunities for the treatment of enterohepatic and metabolic disorders.

EXPERIMENTAL SECTION

Chemistry. Specific rotations were measured on a Jasco P-2000 polarimeter. High-resolution ESI mass spectra were performed with a Micromass Q-TOF mass spectrometer. NMR spectra were obtained on Varian Inova 400 and Varian Inova 700 NMR spectrometers (¹H at 400 and 700 MHz, ¹³C at 100 MHz) equipped with a Sun hardware and recorded in CDCl₃ ($\delta_{\text{H}} = 7.26$ ppm and $\delta_{\text{C}} = 77.0$ ppm) and CD₃OD ($\delta_{\text{H}} = 3.30$ ppm and $\delta_{\text{C}} = 49.0$ ppm). *J* values are in hertz, and chemical shifts (δ) are reported in ppm and referenced to CHCl₃ and CHD₂OD as internal standards. HPLC was performed using a Waters model 510 pump equipped with Waters Rheodine injector and a differential refractometer, model 401. Reaction progress was monitored via thin-layer chromatography (TLC) on Alugram silica gel G/UV254 plates. Silica gel MN Kieselgel 60 (70–230 mesh) from Macherey-Nagel Company was used for column chromatography. All chemicals were obtained from Sigma-Aldrich, Inc. Solvents and reagents were used as supplied from commercial sources with the following exceptions. Tetrahydrofuran, dichloromethane, diisopropylamine, and triethylamine were distilled from calcium hydride immediately prior to use. Methanol was dried from magnesium methoxide as follows. Magnesium turnings (5 g) and iodine (0.5 g) are refluxed in a small (50–100 mL) quantity of methanol until all of the magnesium has reacted. The mixture is diluted (up to 1 L) with reagent grade methanol, refluxed for 2–3 h, and then distilled under nitrogen. All reactions were carried out under argon atmosphere using flame-dried glassware. The purity of all of the intermediates, checked by ¹H NMR, was greater than 95%. The purity of tested compounds was determined to be always greater than 95% by analytical HPLC analysis as reported for each compound.

Compounds **4** and **5** were prepared as previously reported.^{27,28}

Methyl 6 α -Ethyl-3 α -hydroxy-7-keto-5 β -cholan-24-oate (**6**).

A solution of methyl 3 α -hydroxy-6-ethyliden-7-keto-5 β -cholan-24-oate **5** (1.3 g, 3.06 mmol) in dry THF/dry MeOH (50 mL, 1:1 v/v) was hydrogenated in the presence of palladium, 5 wt %, on activated carbon (50 mg). The flask was evacuated and flushed first with argon and then with hydrogen. The mixture was stirred at room temperature under H₂ for 8 h. The catalyst was filtered through Celite, and the recovered filtrate was concentrated under vacuum to give **6** (1.13 g, quantitative yield). An analytic sample was obtained by silica gel chromatography, eluting with hexane/EtOAc 8:2 and 0.5% of triethylamine. [α]_D²⁵ -3.7 (*c* 0.5, CHCl₃). Selected ¹H NMR (400 MHz, CDCl₃): δ 3.67 (3H, s), 3.57 (1H, m), 2.57 (1H, t, *J* = 11.5 Hz), 2.37 (1H, m), 2.24 (1H, dd, *J* = 6.6, 9.6 Hz), 2.20 (1H, m), 1.22 (3H, s), 0.93 (3H, d, *J* = 6.2 Hz), 0.85 (3H, t, *J* = 7.3 Hz), 0.67 (3H, s). ¹³C NMR (100 MHz, CDCl₃): δ 215.1, 178.4, 71.6, 56.3, 51.3, 50.6, 50.4, 47.5, 46.4, 44.4, 43.8, 40.4, 38.2, 36.6, 36.3, 35.2, 32.4, 32.0, 30.6, 29.3, 25.8, 23.5 (2C), 22.8, 18.8, 12.5, 12.0. HRMS-ESI *m/z* 433.3323 [*M* + H⁺], C₂₇H₄₅O₄ requires 433.3318.

6 α -Ethyl-3 α -hydroxy-7-keto-5 β -cholan-24-oic Acid (**7**).

Compound **6** (1.1 g, 2.5 mmol) was hydrolyzed with a methanol solution of sodium hydroxide (5%, 30 mL) in H₂O (6 mL) overnight under reflux. The resulting solution was then concentrated under vacuum, diluted with water, acidified with HCl, 6 N, and extracted with ethyl acetate (3 \times 50 mL). The collected organic phases were washed with brine, dried over anhydrous Na₂SO₄, and evaporated under reduced pressure to give **7** in quantitative yield (1.1 g). An analytic sample was obtained by silica gel chromatography, eluting with CH₂Cl₂/MeOH 95:5. [α]_D²⁵ -21.5 (*c* 0.35, CH₃OH). Selected ¹H NMR (400 MHz, CD₃OD): δ 3.46 (1H, m), 2.83 (1H, dd, *J* = 13.0, 5.5 Hz), 2.50 (1H, t, *J* = 11.2 Hz), 2.34 (1H, m), 2.20 (1H, m), 1.22 (3H, s), 0.96 (3H, d, *J* = 6.6 Hz), 0.81 (3H, t, *J* = 7.3 Hz), 0.71 (3H, s). ¹³C NMR (100 MHz, CD₃OD): δ 215.5, 187.0, 71.7, 56.4, 53.3, 52.2, 51.2, 50.5, 45.4, 43.8, 40.4, 36.8, 36.6, 35.3, 32.6, 32.3, 32.0, 30.6, 29.3, 25.6, 23.9, 23.0, 20.8,

18.8, 12.5, 12.3. HRMS-ESI m/z 419.3164 $[M + H^+]$, $C_{26}H_{43}O_4$ requires 419.3161.

6 α -Ethyl-3 α -formyloxy-7-keto-5 β -cholan-24-oic Acid (8). A solution of 7 (1.0 g, 2.6 mmol) in 30 mL of 90% formic acid containing 90 μ L of 70% perchloric acid was stirred at 47–50 °C for 6 h. The temperature of the heating bath was lowered to 40 °C. Then 24 mL of acetic anhydride was added over 10 min, and the mixture was stirred for 10 min more. The solution was cooled to room temperature, poured into 50 mL of water, and extracted with diethyl ether. The organic layers were washed with water to neutrality, dried over Na_2SO_4 , and evaporated to give 940 mg of 8 (81%). An analytic sample was obtained by silica gel chromatography, eluting with $CH_2Cl_2/MeOH$ 95:5. $[\alpha]_D^{25}$ –25.9 (c 0.56, CH_3OH). Selected 1H NMR (400 MHz, $CDCl_3$): δ 7.99 (1H, s), 4.79 (1H, m), 2.71 (1H, dd, $J = 5.9, 12.8$ Hz), 1.29 (3H, s), 0.93 (3H, d, $J = 6.3$ Hz), 0.80 (3H, t, $J = 7.2$ Hz), 0.66 (3H, s). ^{13}C NMR (100 MHz, $CDCl_3$): δ 212.5, 180.0, 160.6, 73.2, 54.8, 51.9, 50.6, 49.9, 48.9, 43.6, 42.6, 38.9, 35.7, 35.1, 33.8, 30.9, 30.7, 30.3, 28.2, 27.6, 25.9, 24.5, 23.4, 21.8, 18.8, 12.0, 11.9. HRMS-ESI m/z 447.3116 $[M + H^+]$, $C_{27}H_{43}O_5$ requires 447.3110.

6 α -Ethyl-3 α -formyloxy-7-keto-24-nor-5 β -cholan-23-nitrile (9). Crude 8 (930 mg, 2.08 mmol), 6.7 mL of cold trifluoroacetic acid, and 1.8 mL (15.6 mmol) of trifluoroacetic anhydride were stirred at 0–5 °C until dissolution. Sodium nitrite (435 mg, 6.3 mmol) was added in small portions. After the addition was complete, the reaction mixture was stirred first at 0–5 °C for 1 h, then at 38–40 °C for 2 h. On completion, the mixture was neutralized with NaOH, 2 N, and then the product was extracted with 50 mL of diethyl ether (3 \times 50 mL), followed by washing with brine and dried over anhydrous Na_2SO_4 . The ether was removed under reduced pressure to afford 860 mg of 9 in quantitative yield, which was subjected to the next step without any purification.

6 α -Ethyl-3 α -hydroxy-7-keto-24-nor-5 β -cholan-23-oic Acid (10). Crude compound 9 (860 mg, 2.08 mmol) was refluxed with 30% KOH in ~50 mL of methanol/water, 1:1. After the mixture was stirred for 48 h, the basic aqueous solution was neutralized with HCl, 6 N. Then methanol was evaporated and the residue was extracted with AcOEt (3 \times 50 mL). The combined organic layers were washed with brine, dried, and evaporated to dryness to give white solid residue 10 (723 mg, 86%). An analytic sample was obtained by silica gel chromatography, eluting with $CH_2Cl_2/MeOH$ 95:5. $[\alpha]_D^{25}$ –25.2 (c 0.22, CH_3OH). Selected 1H NMR (400 MHz, CD_3OD): δ 3.46 (1H, m), 2.82 (1H, dd, $J = 6.4, 12.6$ Hz), 1.25 (3H, s), 1.25 (3H, d ovl), 0.81 (3H, t, $J = 7.3$ Hz), 0.74 (3H, s). ^{13}C NMR (100 MHz, CD_3OD): δ 215.7, 177.6, 71.7, 56.3, 53.3, 51.2, 50.6, 50.5, 45.3, 43.8, 42.5, 40.4, 36.8, 35.3, 35.0, 32.6, 30.5, 29.4, 25.6, 23.9, 22.9, 20.9, 19.6, 12.5, 12.3. HRMS-ESI m/z 405.3008 $[M + H^+]$, $C_{25}H_{41}O_4$ requires 405.3005.

Methyl 6 α -Ethyl-3 α , 7 α -dihydroxy-24-nor-5 β -cholan-23-oate (11). Compound 10 (715 mg, 1.7 mmol) was dissolved in a solution of tetrahydrofuran/water (50 mL, 4/1 v/v) and treated at 0 °C with $NaBH_4$ (320 mg, 8.5 mmol). After 1 h, water and MeOH were added dropwise during a period of 15 min at 0 °C with effervescence being observed. Then after evaporation of the solvents, the residue was diluted with water, acidified with HCl, 1 N, and extracted with AcOEt (3 \times 50 mL). The combined organic phases were washed with brine, dried over anhydrous Na_2SO_4 , and evaporated under reduced pressure. The crude residue was purified by flash chromatography on silica gel, using dichloromethane/methanol, 9:1, as eluent, to afford 640 mg of 3 $\alpha,7\alpha$ -dihydroxy-6 α -ethyl-24-nor-5 β -cholan-23-oic acid (93% yield). $[\alpha]_D^{25}$ +3.7 (c 1.48, CH_3OH). Selected 1H NMR (400 MHz, CD_3OD): δ 3.62 (1H, br s), 3.30 (1H, m ovl), 0.97 (3H, d, $J = 7.9$ Hz), 0.88 (3H, s), 0.87 (3H, t ovl), 0.70 (3H, s). ^{13}C NMR (100 MHz, CD_3OD): δ 177.8, 73.2, 71.2, 57.5, 51.7, 46.9, 43.9, 43.8, 42.5, 41.6, 41.0, 36.7, 35.1, 34.5, 34.4, 31.3, 29.4, 24.6, 23.8, 23.5, 21.9, 19.6, 12.3, 12.0. HRMS-ESI m/z 407.3166 $[M + H^+]$, $C_{25}H_{43}O_4$ requires 407.3161.

The above compound (640 mg, 1.6 mmol) was dissolved in 50 mL of dry methanol and treated with *p*-toluenesulfonic acid (1.5 g, 8.0 mmol). The solution was left to stand at room temperature overnight. The mixture was quenched by addition of $NaHCO_3$ solution until neutrality. Most of the solvent was evaporated, and the residue was extracted with EtOAc. The combined extract was washed with brine,

dried with Na_2SO_4 , and evaporated to give 11 as an amorphous solid (645 mg, 96%). An analytic sample was obtained by silica gel chromatography, eluting with hexane/EtOAc 6:4. $[\alpha]_D^{25}$ +0.95 (c 0.96, $CHCl_3$). Selected 1H NMR (400 MHz, CD_3OD): δ 3.61 (3H, s), 3.62 (1H, s ovl), 3.28 (1H, m), 0.95 (3H, d, $J = 6.9$ Hz), 0.88 (3H, s), 0.87 (3H, t, $J = 7.2$ Hz), 0.69 (3H, s). ^{13}C NMR (100 MHz, CD_3OD): δ 175.7, 73.2, 71.2, 57.8, 51.8, 51.6, 46.9, 43.9, 43.8, 43.1, 42.3, 41.5, 41.0, 36.7, 35.2, 35.1, 34.4, 31.2, 29.3, 24.5, 23.8, 23.5, 21.9, 19.6, 12.3, 12.0. HRMS-ESI m/z 421.3322 $[M + H^+]$, $C_{26}H_{45}O_4$ requires 421.3318.

Methyl 3 $\alpha,7\alpha$ -Di(*tert*-butyldimethylsilyloxy)-6 α -ethyl-24-nor-5 β -cholan-23-oate (12). To a solution of 11 (600 mg, 1.4 mmol) in 20 mL of CH_2Cl_2 at 0 °C were added 2,6-lutidine (14.3 mmol, 1.6 mL) and *tert*-butyl dimethylsilyltrifluoromethanesulfonate (4.2 mmol, 960 μ L). After the mixture was stirred for 24 h at 0 °C, the reaction was quenched by addition of aqueous $NaHSO_4$ (1 M, 50 mL). The layers were separated, and the aqueous phase was extracted with CH_2Cl_2 (3 \times 50 mL). The combined organic layers were washed with $NaHSO_4$, water, saturated aqueous $NaHCO_3$, and brine. Purification by flash chromatography on silica gel using hexane/ethyl acetate, 9:1, and 0.5% of triethylamine as eluent gave 12 (722 mg, 78%) as a clear, colorless oil. $[\alpha]_D^{25}$ +2.44 (c 0.62, $CHCl_3$). Selected 1H NMR (400 MHz, $CDCl_3$): δ 3.69 (1H, br s), 3.48 (3H, s), 3.40 (1H, m), 1.02 (3H, d, $J = 6.3$ Hz), 0.90 (3H, t, $J = 7.3$ Hz), 0.89 (3H, s), 0.86 (18H, s), 0.70 (3H, s), 0.042 (12H, s). ^{13}C NMR (100 MHz, $CDCl_3$): δ 176.3, 74.1, 72.9, 56.0, 51.6, 51.6, 49.4, 45.1, 43.2, 42.4, 41.9, 41.5, 40.8, 35.7, 34.9, 34.1, 33.9, 31.8, 31.3, 26.7, 26.6, 25.7 (3C), 25.6 (3C), 24.4, 24.0, 23.0, 19.3, 18.8, 12.0, 11.9, –3.0 (2C), –2.8 (2C). HRMS-ESI m/z 641.5051 $[M + H^+]$, $C_{38}H_{73}O_4Si_2$ requires 641.5047.

6 α -Ethyl-3 $\alpha,7\alpha$ -dihydroxy-24-nor-5 β -cholan-23yl-23-triethylammonium Sulfate 1. Dry methanol (133 μ L, 3.3 mmol) and $LiBH_4$ (1.7 mL, 2 M in THF, 3.3 mmol) were added to a solution of 12 (722 mg, 1.1 mmol) in dry THF (15 mL) at 0 °C under argon, and the resulting mixture was stirred for 8 h at 0 °C. The mixture was quenched by addition of NaOH (1 M, 2.2 mL) and then allowed to warm to room temperature. Ethyl acetate was added, and the separated aqueous phase was extracted with ethyl acetate (3 \times 30 mL). The combined organic phases were washed with water, dried (Na_2SO_4), and concentrated. Purification by silica gel (*n*-hexane/ethyl acetate 8:2) gave C23 alcohol derivative as a colorless oil (650 mg, 95%). $[\alpha]_D^{25}$ –0.25 (c 0.5, CH_3OH). Selected 1H NMR (400 MHz, $CDCl_3$): δ 3.70 (1H, m), 3.67 (1H, br s), 3.60 (1H, m), 3.37 (1H, m), 0.94 (3H, d, $J = 6.4$ Hz), 0.87 (3H, s), 0.87 (3H, t ovl), 0.86 (18H, s), 0.66 (3H, s), 0.042 (12H, s). ^{13}C NMR (100 MHz, $CDCl_3$): δ 73.6, 71.2, 61.0, 56.6, 50.8, 45.6, 43.0, 41.5, 40.3, 39.9, 36.0, 35.8, 34.4, 33.5, 33.2 (2C), 31.3, 28.6, 26.2 (7C), 23.9, 23.4, 22.5, 21.0, 19.0, 12.0, 11.8, –4.3 (2C), –4.4 (2C). HRMS-ESI m/z 621.5093 $[M + H^+]$, $C_{37}H_{73}O_3Si_2$ requires 621.5098.

The triethylamine–sulfur trioxide complex (906 mg, 5 mmol) was added to a solution of C23 alcohol (620 mg, 1 mmol) in DMF dry (7 mL) under an argon atmosphere, and the mixture was stirred at 95 °C for 24 h. The solution was then concentrated under vacuum. To the solid dissolved in methanol (30 mL) was added three drops of HCl, 37% v/v, and the mixture was stirred for 5 h at room temperature. At the end of reaction, silver carbonate was added to precipitate chloride. Then the reaction mixture was centrifuged and the supernatant was concentrated in vacuo. The residue was poured over a RP18 column. The fraction eluted with $H_2O/MeOH$ (1:1) gave compound 1 as a white solid (500 mg, 87%). A sample (20 mg) was subjected to purification by HPLC on a Nucleodur 100-5 C18 (5 μ m, 10 mm i.d. \times 250 mm) with $MeOH/H_2O$ (65:35) as eluent (flow rate 3 mL/min ($t_R = 24.8$ min)). $[\alpha]_D^{25}$ +2.9 (c 0.17, CH_3OH). 1H and ^{13}C NMR data in CD_3OD are given in Table S1. HR ESIMS m/z 471.2775 $[M - Na]$, $C_{25}H_{43}O_6S$ requires 471.2780.

Compound 13. To a solution of 11 (30 mg, 0.07 mmol) in dry THF (5 mL) at 0 °C, dry methanol (20 μ L, 0.5 mmol) and $LiBH_4$ (250 μ L, 2 M in THF, 0.5 mmol) were added. The resulting mixture was stirred for 8 h at 0 °C. The mixture was quenched by addition of NaOH (1 M, 240 μ L), and then ethyl acetate was added. The separated aqueous phase was extracted with ethyl acetate (3 \times 30 mL).

The combined organic phases were washed with water, dried (Na_2SO_4), and concentrated. Purification by silica gel ($\text{CH}_2\text{Cl}_2/\text{MeOH}$ 9:1) gave triol derivative as a white solid (27 mg, quantitative yield). $[\alpha]_{25}^D +1.97$ (*c* 0.5, CH_3OH). Selected ^1H NMR (400 MHz, CDCl_3): δ 3.67 (1H, br s), 3.60 (2H, m), 3.43 (1H, m), 0.93 (3H, d, *J* = 6.6 Hz), 0.88 (3H, s), 0.87 (3H, t, *J* = 7.1 Hz), 0.67 (3H, s). ^{13}C NMR (100 MHz, CDCl_3): δ 73.2, 71.2, 60.8, 57.9, 51.7, 51.6, 46.9, 43.9, 43.1, 41.5, 41.0, 39.8, 36.7, 36.6, 34.5, 34.4, 34.2, 31.2, 29.3, 24.5, 23.7, 23.5, 21.9, 19.5, 19.3, 12.2, 12.0. HRMS-ESI *m/z* 393.3367 [*M* + H^+], $\text{C}_{25}\text{H}_{45}\text{O}_3$ requires 393.3369.

Triethylamine–sulfur trioxide complex (127 mg, 0.7 mmol) was added to triol (27 mg, 0.07 mmol) in DMF dry (10 mL) under an argon atmosphere, and the mixture was stirred at 95 °C for 48 h. The reaction mixture was quenched with water (1.6 mL), and the solution was poured over a C18 silica gel column to remove excess $\text{Et}_3\text{N}\cdot\text{SO}_3$. The fraction eluted with $\text{H}_2\text{O}/\text{MeOH}$ (9:1) gave a mixture, which was further purified by HPLC on a Nucleodur 100-5 C18 (5 μm , 10 mm i.d. \times 250 mm) with $\text{MeOH}/\text{H}_2\text{O}$ (35:65) as eluent (flow rate 3 mL/min) to give compound 13 as a white solid (47 mg, 72%). $[\alpha]_{25}^D -2.3$ (*c* 0.24, CH_3OH). Selected ^1H NMR (400 MHz, CD_3OD): δ 4.62 (1H, br s), 4.11 (1H, m), 4.03 (2H, m), 3.19 (18H, q, *J* = 7.2 Hz), 1.30 (27H, t, *J* = 7.2 Hz), 0.99 (3H, d, *J* = 6.5 Hz), 0.96 (3H, s), 0.93 (3H, t, *J* = 7.4 Hz), 0.71 (3H, s). HR ESIMS *m/z* 833.4322 [*M* – Et_3NH], $\text{C}_{37}\text{H}_{73}\text{N}_2\text{O}_{12}\text{S}_3$ requires 833.4326.

Chenodeoxycholan Sulfate Derivative Synthesis. Methyl 3 α ,7 α -Dihydroxy-5 β -cholan-24-oate (14). A mixture of CDCA (3, 100 mg, 0.25 mmol) and *p*-toluenesulfonic acid (237 mg, 1.25 mmol) in dry methanol (10 mL) was left to stand at room temperature for 1 h. The mixture was quenched by addition of NaHCO_3 solution until neutrality. Most of the solvent was evaporated, and the residue was extracted with EtOAc . The combined extract was washed with brine, dried with Na_2SO_4 , and evaporated to give the desired methyl ester as colorless amorphous solids (102 mg, quantitative yield). An analytic sample was obtained by silica gel chromatography, eluting with $\text{CH}_2\text{Cl}_2/\text{MeOH}$ 95:5. $[\alpha]_{25}^D +7.81$ (*c* 2.33, CHCl_3). Selected ^1H NMR (400 MHz, CDCl_3): δ 3.73 (1H, br s), 3.57 (3H, s), 3.30 (1H, m ovl), 2.26 (1H, m), 2.13 (1H, m), 0.84 (3H, d, *J* = 6.0 Hz), 0.82 (3H, s), 0.60 (3H, s). ^{13}C NMR (100 MHz, CDCl_3): δ 174.4, 71.2, 67.6, 55.3, 51.0, 49.8, 42.0, 41.1, 39.2, 38.8 (2C), 34.9, 34.8, 34.5, 34.2, 32.3, 30.5, 30.4, 29.9, 27.7, 23.0, 22.3, 20.1, 17.7, 11.2. HRMS-ESI *m/z* 407.3165 [*M* + H^+], $\text{C}_{25}\text{H}_{43}\text{O}_4$ requires 407.3161.

3 α ,7 α ,24-5 β -Cholantriol (16). Methyl ester 14 (100 mg, 0.25 mmol) was dissolved in dry THF (5 mL) at 0 °C in the presence of dry methanol (70 μL , 0.84 mmol) and LiBH_4 (875 μL , 2 M in THF, 1.75 mmol). After 8 h, a solution of 1 M NaOH (500 μL) was added and then allowed to warm to room temperature. Ethyl acetate was added, and the separated aqueous phase was extracted with ethyl acetate (3 \times 30 mL). The combined organic phases were washed with water, dried (Na_2SO_4), and concentrated. Purification by silica gel ($\text{CH}_2\text{Cl}_2/\text{MeOH}$ 95:5) gave triol derivative 16 as a colorless oil (90 mg, 96%). $[\alpha]_{25}^D +0.82$ (*c* 2.07, CH_3OH). Selected ^1H NMR (400 MHz, CDCl_3): δ 3.80 (1H, br s), 3.56 (2H, m), 3.40 (1H, m), 0.91 (3H, d, *J* = 6.0 Hz), 0.87 (3H, s), 0.63 (3H, s). ^{13}C NMR (100 MHz, CDCl_3): δ 71.8, 68.4, 63.2, 56.0, 50.3, 42.5, 41.5, 39.6, 39.3 (2C), 35.5, 35.3, 34.9, 34.5, 32.8, 30.5 (2C), 29.3, 28.2, 23.6, 22.7, 20.5, 18.6, 11.7. HRMS-ESI *m/z* 379.3216 [*M* + H^+], $\text{C}_{24}\text{H}_{43}\text{O}_3$ requires 379.3212.

3 α ,7 α -Dihydroxy-5 β -cholan-24-yl-24-sodium Sulfate (18). At a solution of triol 16 (40 mg, 0.1 mmol) in DMF dry (3 mL) was added triethylamine–sulfur trioxide complex (36 mg, 0.2 mmol) under an argon atmosphere, and the mixture was stirred at 95 °C for 1 h. Most of the solvent was evaporated, and the residue was poured over a RP18 column to remove excess $\text{SO}_3\cdot\text{NEt}_3$. The fraction eluted with $\text{H}_2\text{O}/\text{MeOH}$ 1:1 gave a mixture that was further purified by HPLC on a Nucleodur 100-5 C18 (5 μm , 4.6 mm i.d. \times 250 mm) with $\text{MeOH}/\text{H}_2\text{O}$ (65:35) as eluent (flow rate 1 mL/min) to give 35 mg (73%) of compound 18 (t_R = 11.2 min). $[\alpha]_{25}^D +4.93$ (*c* 0.05, CH_3OH). Selected ^1H NMR (400 MHz, CD_3OD): δ 3.95 (2H, t, *J* = 6.4 Hz), 3.78 (1H, br s), 3.30 (1H, m ovl), 0.96 (3H, d ovl), 0.95 (3H, s), 0.70 (3H, s). HR ESIMS *m/z* 457.2627 [*M* – Na], $\text{C}_{24}\text{H}_{41}\text{O}_6\text{S}$ requires 457.2624.

5 β -Cholan-3 α ,7 α ,24-tryl-3,7,24-sodium Trisulfate (20). The triethylamine–sulfur trioxide complex (91 mg, 0.5 mmol) was added to a solution of triol 16 (40 mg, 0.1 mmol) in dry DMF (3 mL) under an argon atmosphere, and the mixture was stirred at 95 °C for 3 h. Most of the solvent was evaporated, and the residue was poured over a RP18 column to remove excess $\text{SO}_3\cdot\text{NEt}_3$. The fraction eluted with $\text{H}_2\text{O}/\text{MeOH}$, 9:1, gave a mixture that was further purified by HPLC on a Nucleodur 100-5 C18 (5 μm , 4.6 mm i.d. \times 250 mm) with $\text{MeOH}/\text{H}_2\text{O}$ (35:65) as eluent (flow rate 1 mL/min) to give 20 (44 mg, t_R = 8 min, 65%). $[\alpha]_{25}^D +4.78$ (*c* 0.12, CH_3OH). ^1H NMR (400 MHz, CD_3OD): δ 4.45 (1H, br s), 4.15 (1H, m), 3.95 (2H, t, *J* = 6.5 Hz), 2.35 (1H, d, *J* = 12.5 Hz), 2.3 (1H, d, *J* = 14.0 Hz), 0.97 (3H, d ovl), 0.97 (3H, s), 0.70 (3H, s). HR ESIMS *m/z* 661.1395 [*M* – Na], $\text{C}_{24}\text{H}_{39}\text{Na}_2\text{O}_{12}\text{S}_3$ requires 661.1399.

The same sequence of reactions and purification procedure was carried out on 6 α -ethylchenodeoxycholic acid (15) to give a mixture of compounds 19 and 21. Purification by HPLC on a Nucleodur 100-5 C18 (5 μm , 4.6 mm i.d. \times 250 mm) with $\text{MeOH}/\text{H}_2\text{O}$ (65:35) as eluent (flow rate 1 mL/min) gave compound 19 (t_R = 22.0 min) as a white solid (15 mg). Purification by HPLC on a Nucleodur 100-5 C18 (5 μm , 4.6 mm i.d. \times 250 mm) with $\text{MeOH}/\text{H}_2\text{O}$ (35:65) as eluent (flow rate 1 mL/min) gave compound 21 (t_R = 24.0 min) as a white solid (27 mg).

6 α -Ethyl-3 α ,7 α -dihydroxy-5 β -cholan-24-yl-24-sodium Sulfate (19). $[\alpha]_{25}^D +3.18$ (*c* 0.51, CH_3OH). Selected ^1H NMR (400 MHz, CD_3OD): δ 3.96 (2H, t, *J* = 6.3 Hz), 3.65 (1H, br s), 3.30 (1H, m ovl), 0.97 (3H, d, *J* = 6.5 Hz), 0.92 (3H, s), 0.90 (3H, t, *J* = 7.0 Hz), 0.70 (3H, s). ^{13}C NMR (100 MHz, CD_3OD): δ 72.2, 70.9, 69.6, 56.4, 50.5, 45.9, 42.5, 41.1, 39.9, 39.6, 35.7, 35.6 (2C), 35.4, 33.4, 32.0, 31.9, 29.3, 28.2, 23.6 (2C), 23.1, 20.5, 18.9, 12.2, 11.9. HR ESIMS *m/z* 485.2935 [*M* – Na], $\text{C}_{26}\text{H}_{45}\text{O}_6\text{S}$ requires 485.2937.

6 α -Ethyl-5 β -cholan-3 α ,7 α ,24-tryl-3,7, 24-sodium Trisulfate (21). $[\alpha]_{25}^D -1.9$ (*c* 0.23, CH_3OH). Selected ^1H NMR (400 MHz, CD_3OD): δ 4.55 (1H, br s), 4.09 (1H, m), 3.96 (2H, t, *J* = 6.0 Hz), 0.97 (3H, d, *J* = 6.4 Hz), 0.92 (3H, s), 0.90 (3H, t, *J* = 7.0 Hz), 0.70 (3H, s). HR ESIMS *m/z* 689.1715 [*M* – Na], $\text{C}_{26}\text{H}_{43}\text{Na}_2\text{O}_{12}\text{S}_3$ requires 689.1712.

Bis-homochenodeoxycholan Sulfate Derivatives. 3 α ,7 α -Di-(tert-butyl)dimethylsilyloxy-5 β -cholan-24-ol (22). 2,6-Lutidine (290 μL , 2.5 mmol) and *tert*-butyl dimethylsilyltrifluoromethanesulfonate (171 μL , 0.75 mmol) were added at 0 °C to a solution of methyl ester 14 (100 mg, 0.25 mmol) in 10 mL of CH_2Cl_2 . After the mixture was stirred for 2 h at 0 °C, the reaction was quenched by addition of aqueous NaHSO_4 (1 M, 50 mL). The layers were separated, and the aqueous phase was extracted with CH_2Cl_2 (3 \times 50 mL). The combined organic layers were washed with NaHSO_4 , water, saturated aqueous NaHCO_3 , and brine. Purification by flash chromatography on silica gel using hexane/ethyl acetate, 99:1, and 0.5% of triethylamine as eluent gave the corresponding methyl ester (131 mg, 83%) as a clear, colorless oil. To a solution of methyl ester (100 mg, 0.16 mmol) in dry THF (5 mL) at 0 °C were added dry methanol (45 μL , 1.12 mmol) and LiBH_4 (560 μL , 2 M in THF, 1.12 mmol). The resulting mixture was stirred for 3 h at 0 °C. The mixture was quenched by addition of 1 M NaOH (320 μL) and then ethyl acetate. The organic phase was washed with water, dried (Na_2SO_4), and concentrated. Purification by silica gel (hexane/ethyl acetate 8:2) gave compound 22 as a white solid (97 mg, quantitative yield). $[\alpha]_{25}^D +7.47$ (*c* 0.12, CHCl_3). Selected ^1H NMR (400 MHz, CDCl_3): δ 3.82 (1H, br s), 3.47 (2H, t, *J* = 6.5 Hz), 3.41 (1H, m), 0.93 (3H, d, *J* = 6.0 Hz), 0.88 (9H, s), 0.88 (3H, s ovl), 0.86 (9H, s), 0.65 (3H, s), 0.08 (6H, s), 0.04 (6H, s). ^{13}C NMR (100 MHz, CDCl_3): δ 72.8, 69.7, 63.4, 56.3, 50.1, 42.5, 42.0, 40.7, 40.6, 39.8, 36.0, 35.8, 35.2, 34.8, 32.4, 32.2, 31.2, 29.7 (3C), 28.3, 26.3 (3C), 26.0 (3C), 24.1, 23.0, 20.7, 18.8, 12.0, –2.2, –4.4, –4.5, –5.4. HRMS-ESI *m/z* 607.4946 [*M* + H^+], $\text{C}_{36}\text{H}_{71}\text{O}_3\text{Si}_2$ requires 607.4942.

Ethyl 3 α , 7 α -Di-(tert-butyl)dimethylsilyloxy-25,26-bis-homo-5 β -chol-24-en-26-oate (23). DMSO (4.18 mL, 0.75 mmol) was added dropwise for 5 min to a solution of oxalyl chloride (14.7 mL, 0.37 mmol) in dry dichloromethane (5 mL) at –78 °C under argon atmosphere. After 30 min, a solution of 22 (90 mg, 0.15 mmol) in dry

CH_2Cl_2 (2 mL) was added dropwise and the mixture was stirred at -78°C . After 30 min, Et_3N dry (6.83 mL, 0.75 mmol) was added dropwise to the solution and the mixture was allowed to warm to room temperature. After 1 h, the reaction was quenched by addition of aqueous NaHSO_4 (1 M, 50 mL). The layers were separated, and the aqueous phase was extracted with CH_2Cl_2 (3×50 mL). The combined organic layers were washed with saturated aqueous NaHSO_4 , saturated aqueous NaHCO_3 , and brine. The organic phase was then dried over Na_2SO_4 and concentrated to give the corresponding aldehyde (90 mg, quantitative yield) as a colorless oil, which was used without any further purification. To a solution of aldehyde (0.15 mmol) in THF dry (10 mL) was added LiOH (250 mg, 10.5 mmol) and TEPA (triethylphosphonoacetate, 2.07 mL, 10.5 mmol). The reaction mixture was stirred for 45 min at room temperature and then quenched with water (10 mL). The mixture was then extracted with EtOAc (3×30 mL), and the organic phase was concentrated in vacuo. Flash chromatography (hexane/EtOAc, 99:1) afforded pure **23** (92 mg, 91% over two steps). $[\alpha]_{25}^{\text{D}} +3.31$ (c 0.5, CHCl_3). Selected ^1H NMR (400 MHz, CDCl_3): δ 6.93 (1H, dt, $J = 5.1, 15.6$ Hz), 5.78 (1H, d, $J = 15.6$ Hz), 4.1 (2H, m), 3.77 (1H, br s), 3.38 (1H, m), 0.91 (3H, d ovl), 0.90 (9H, s), 0.90 (3H, s ovl), 0.87 (9H, s), 0.61 (3H, s), 0.06 (6H, s), 0.03 (6H, s). ^{13}C NMR (100 MHz, CDCl_3): δ 178.5, 149.8, 120.8, 72.5, 69.5, 59.9, 55.8, 49.9, 42.3, 41.8, 40.5, 40.4, 39.5, 35.6 (2C), 35.0, 34.6, 34.3, 32.2, 30.9, 29.6, 29.1 (2C), 28.0, 26.0 (3C), 25.8 (3C), 23.8, 22.7, 20.5, 18.4, 14.2, 12.0, -2.4, -4.5, -4.6, -5.6. HRMS-ESI m/z 675.5207 $[\text{M} + \text{H}^+]$, $\text{C}_{40}\text{H}_{75}\text{O}_4\text{Si}_2$ requires 675.5204.

Ethyl 25,26-Bis-homo-3 α ,7 α -dihydroxy-5 β -cholan-26-oate (24). Compound **23** (90 mg, 0.13 mmol) and THF dry (15 mL) were mixed and deoxygenated with flowing nitrogen for 5 min. The catalyst $\text{Pd}(\text{OH})_2$ (5 mg, mmol), 20 wt % on carbon (Degussa type), was added. The mixture was transferred to a standard PARR apparatus and flushed with nitrogen and then with hydrogen several times. The apparatus was shacked under 50 psi of H_2 . After 2 h, the reaction was complete. The catalyst was filtered through Celite, and the recovered filtrate was concentrated under vacuum to afford 92 mg of ethyl ester in quantitative yield, which was subjected to the next step without any purification. To the ethyl ester dissolved in ethanol (30 mL) was added 1 mL of HCl, 37% v/v, and the mixture was stirred for 5 h at room temperature. At the end of reaction, silver carbonate was added to precipitate chloride. Then the reaction mixture was centrifuged and the supernatant was concentrated in vacuo to give the desired ethyl ester **24** (50 mg, 81% over two steps) as a colorless amorphous solid. An analytic sample was obtained by silica gel chromatography, eluting with $\text{CH}_2\text{Cl}_2/\text{MeOH}$ 95:5. $[\alpha]_{25}^{\text{D}} +6.72$ (c 0.25, CHCl_3). Selected ^1H NMR (400 MHz, CDCl_3): δ 4.1 (2H, q, $J = 7.0$ Hz), 3.8 (1H, br s), 3.38 (1H, m), 2.29 (2H, t, $J = 6.7$ Hz), 1.24 (3H, t, $J = 7.0$ Hz), 0.94 (3H, d, $J = 6.6$ Hz), 0.92 (3H, s), 0.68 (3H, s). ^{13}C NMR (100 MHz, CDCl_3): δ 175.4, 72.8, 69.0, 61.4, 57.4, 51.5, 43.6, 43.1, 41.0, 40.7, 40.3, 37.0, 36.7, 36.5, 35.8, 35.2, 34.8, 34.0, 31.3, 29.3, 26.6, 26.5, 24.6, 23.5, 21.8, 19.3, 14.6, 12.3. HRMS-ESI m/z 449.3635 $[\text{M} + \text{H}^+]$, $\text{C}_{28}\text{H}_{49}\text{O}_4$ requires 449.3631.

25,26-Bis-homo-3 α ,7 α ,26-5 β -cholantriol (25). Ethyl ester **24** (40 mg, 0.09 mmol) was reduced with LiBH_4 (2 M in THF dry, 135 μL , 0.27 mmol) and dry MeOH (11 μL , 0.27 mmol) in dry THF at 0°C for 5 h. The mixture was quenched by addition of 1 M NaOH solution (180 μL), and then ethyl acetate was added. The organic phase was washed with water, dried (Na_2SO_4), and concentrated. Purification by silica gel ($\text{CH}_2\text{Cl}_2/\text{MeOH}$ 9:1) gave compound **25** as a white solid (28 mg, 77%). $[\alpha]_{25}^{\text{D}} +15.0$ (c 0.32, CH_3OH). Selected ^1H NMR (400 MHz, CDCl_3): δ 3.82 (1H, br s), 3.61 (2H, t, $J = 6.6$ Hz), 3.43 (1H, m), 0.89 (3H, d, $J = 6.0$ Hz), 0.88 (3H, s), 0.64 (3H, s). ^{13}C NMR (100 MHz, CDCl_3): δ 71.8, 68.4, 62.8, 56.0, 50.4, 42.5, 41.4, 39.6 (2C), 39.4, 35.8, 35.6, 35.2, 35.0, 34.5, 32.8 (2C), 30.5, 28.2, 26.1, 25.8, 23.6, 22.7, 20.5, 18.6, 11.6. HRMS-ESI m/z 407.3523 $[\text{M} + \text{H}^+]$, $\text{C}_{26}\text{H}_{47}\text{O}_4$ requires 407.3525.

25,26-Bis-homo-3 α ,7 α -dihydroxy-5 β -cholan-26-yl-26-sodium Sulfate (26) and 25,26-Bis-homo-5 β -cholan-3 α , 7 α , 26-tryl-3,7,26-sodium Trisulfate (27). The triethylamine-sulfur trioxide complex (132 mg, 0.7 mmol) was added to a solution of

triol **25** (28 mg, 0.07 mmol) in DMF dry (3 mL) under an argon atmosphere, and the mixture was stirred at 95°C for 3 h. Most of the solvent was evaporated, and the residue was poured over a RP18 column to remove excess $\text{SO}_3\text{-NET}_3$. The fraction eluted with $\text{H}_2\text{O}/\text{MeOH}$ 1:1 gave a mixture that was further purified by HPLC on a Nucleodur 100-5 C18 (5 μm , 4.6 mm i.d. \times 250 mm) with $\text{MeOH}/\text{H}_2\text{O}$ (65:35) as eluent (flow rate 1 mL/min) to give 4 mg of compound **26**.

The fraction eluted with $\text{H}_2\text{O}/\text{MeOH}$ (9:1) gave a mixture that was further purified by HPLC (Nucleodur 100-5 C18, 5 μm , 4.6 mm i.d. \times 250 mm), with $\text{MeOH}/\text{H}_2\text{O}$ (35:65) as eluent (flow rate 1 mL/min), to give 33 mg of compound **27**.

25,26-Bis-homo-3 α ,7 α -dihydroxy-5 β -cholan-26-yl-26-sodium Sulfate (26). $[\alpha]_{25}^{\text{D}} +9.13$ (c 0.05, CH_3OH). Selected ^1H NMR (400 MHz, CD_3OD): δ 3.98 (2H, t, $J = 6.5$ Hz), 3.79 (1H, m), 3.31 (1H, m ovl), 0.95 (3H, d, $J = 6.8$ Hz), 0.93 (3H, s), 0.63 (3H, s). HR ESIMS m/z 485.2939 $[\text{M} - \text{Na}]$, $\text{C}_{26}\text{H}_{45}\text{O}_6\text{S}$ requires 485.2937.

25,26-Bis-homo-5 β -cholan-3 α ,7 α ,26-tryl-3,7,26-sodium Trisulfate (27). $[\alpha]_{25}^{\text{D}} +1.35$ (c 1.13, CH_3OH). Selected ^1H NMR (400 MHz, CD_3OD): δ 4.45 (1H, br s), 4.13 (1H, m), 3.98 (2H, t, $J = 6.5$ Hz), 0.95 (3H, d, $J = 6.6$ Hz), 0.93 (3H, s), 0.69 (3H, s). HR ESIMS m/z 689.1716 $[\text{M} - \text{Na}]$, $\text{C}_{26}\text{H}_{43}\text{Na}_2\text{O}_{12}\text{S}_3$ requires 689.1712.

Ursodeoxycholan Sulfate and Bis-homoursodeoxycholan Sulfate Derivatives. 3 α ,7 β -Di(tert-butylidimethylsilyloxy)-5 β -cholan-24-ol (29). To a solution of methyl 3 α ,7 β -dihydroxy-5 β -cholan-24-oate (2 g, 5 mmol) in CH_2Cl_2 dry (50 mL) was added at 0°C 2,6-lutidine (49 mmol, 5.72 mL) and *tert*-butyl dimethylsilyl-trifluoromethanesulfonate (15 mmol, 3.43 mL). After 2 h, the reaction was quenched by addition of aqueous NaHSO_4 , 1 M. The layers were separated, and the aqueous phase was extracted with CH_2Cl_2 (3×50 mL). The combined organic layers were washed with NaHSO_4 , saturated aqueous NaHCO_3 , and finally water. The organic phase was then dried over Na_2SO_4 and concentrated to give the corresponding methyl ester **28** (3.10 g, quantitative yield) as a colorless oil, which was used without any further purification. Dry methanol (600 μL , 15 mmol) and LiBH_4 (7.50 mL, 2 M in THF, 15 mmol) were added to a solution of methyl ester (3.10 g, 5 mmol) in dry THF (15 mL) at 0°C under argon, and the resulting mixture was stirred for 8 h at 0°C . The mixture was quenched by addition of NaOH (1 M, 10 mL) and then allowed to warm to room temperature. Ethyl acetate was added, and the separated aqueous phase was extracted with ethyl acetate (3×30 mL). The combined organic phases were washed with water, dried (Na_2SO_4), and concentrated. Purification by silica gel (*n*-hexane/ethyl acetate 99:1) gave compound **29** as a colorless oil (2.40 g, 80%). $[\alpha]_{25}^{\text{D}} +21.7$ (c 0.49, CHCl_3). Selected ^1H NMR (400 MHz, CDCl_3): δ 3.61 (2H, m), 3.50 (2H, m), 0.88 (3H, d, ovl), 0.88 (3H, s), 0.88 (9H, s), 0.83 (9H, s), 0.60 (3H, s), 0.003 (6H, s), -0.01 (6H, s). ^{13}C NMR (100 MHz, CDCl_3): δ 72.7, 72.5, 61.0, 55.5, 55.4, 44.0, 43.8, 42.8, 40.0, 39.0, 38.8, 38.0, 37.8, 35.4, 35.1, 34.1, 32.8, 31.8 (2C), 30.8, 28.7, 27.3, 26.4 (3C), 25.9 (3C), 23.5, 21.2, 19.0, 12.1, -2.8 (2C), -4.6 (2C). HRMS-ESI m/z 607.4947 $[\text{M} + \text{H}^+]$, $\text{C}_{36}\text{H}_{70}\text{O}_3\text{Si}_2$ requires 607.4942.

3 α ,7 β -Dihydroxy-5 β -cholan-24-yl-24-sodium Sulfate (30). To a solution of compound **29** (100 mg, 0.16 mmol) in DMF dry (7 mL) was added 58 mg of triethylamine-sulfur trioxide complex (0.32 mmol). The mixture was stirred at 95°C for 4 h. Then the solution was concentrated under vacuum. To the solid dissolved in methanol (30 mL) was added three drops of HCl, 37% v/v, and the mixture was stirred for 3 h at room temperature. At the end of reaction, silver carbonate was added to precipitate chloride. Then the reaction mixture was centrifuged and the supernatant was concentrated in vacuo. The residue was poured over a RP18 column. The fraction eluted with $\text{H}_2\text{O}/\text{MeOH}$ (7:3) gave 53 mg (69% over two steps) of compound **30**. $[\alpha]_{25}^{\text{D}} +15.3$ (c 0.97, CH_3OH). Selected ^1H NMR (400 MHz, CD_3OD): δ 3.96 (2H, t, $J = 6.6$ Hz), 3.48 (2H, m), 0.97 (3H, d, $J = 6.4$ Hz), 0.96 (3H, s), 0.71 (3H, s). ^{13}C NMR (100 MHz, CD_3OD): δ 72.3 (2C), 69.6, 57.0, 56.4, 44.8, 43.0 (2C), 41.2, 40.7, 37.3 (2C), 36.7, 36.0, 35.5, 32.7, 30.6, 29.8, 27.8, 26.5, 23.3, 22.6, 20.0, 12.0. HR ESIMS m/z 457.2621 $[\text{M} - \text{Na}]$, $\text{C}_{24}\text{H}_{41}\text{O}_6\text{S}$ requires 457.2624.

5 β -Cholan-3 α ,7 β ,24-tryl-3,7,24-sodium Trisulfate (31), 7 β -Hydroxy-5 β -cholan-3 α ,24-diyl-3,24-sodium Disulfate (32), and 7 β ,24-Dihydroxy-5 β -cholan-3 α -yl-3-sodium Sulfate (33). To compound 29 (100 mg, 0.16 mmol) dissolved in methanol (30 mL) was added 500 μ L of HCl, 37% v/v, and the mixture was stirred for 2 h at room temperature. At the end of reaction, silver carbonate was added to precipitate chloride. Then the reaction mixture was centrifuged and the supernatant was concentrated in vacuo to give 60 mg (96%) of the desired triol as colorless amorphous solids. An analytic sample was obtained by silica gel chromatography, eluting with CH₂Cl₂/MeOH 95:5.

The triethylamine–sulfur trioxide complex (118 mg, 0.65 mmol) was added to a solution of triol (50 mg, 0.13 mmol) in DMF dry (3 mL). The mixture was stirred at 95 °C for 2 h. Then the solution was concentrated under vacuum. The residue was poured over a RP18 column. The fraction eluted with H₂O/MeOH (99:1) gave a mixture that was further purified by HPLC on a Nucleodur 100-5 C18 (5 μ m, 10 mm i.d. \times 250 mm) with MeOH/H₂O (35:65) as eluent (flow rate 3 mL/min) to give 13 mg of 31 and 8 mg of 32. The fraction eluted with H₂O/MeOH (1:1) gave a mixture that, purified by HPLC on a Nucleodur 100-5 C18 (5 μ m, 10 mm i.d. \times 250 mm) with MeOH/H₂O (65:35) as eluent (flow rate 3 mL/min), afforded 14 mg of 33.

5 β -Cholan-3 α ,7 β ,24-tryl-3,7,24-sodium Trisulfate (31). [α]₂₅^D +20.6 (c 0.08, CH₃OH). ¹H NMR (400 MHz, CD₃OD): δ 4.28 (1H, m), 4.21 (1H, br s), 3.96 (2H, t, *J* = 6.7 Hz), 0.98 (3H, s), 0.97 (3H, d, *J* = 6.8 Hz), 0.71 (3H, s). HR ESIMS *m/z* 661.1395 [M – Na], C₂₄H₃₉Na₂O₁₂S₃ requires 661.1399.

7 β -Hydroxy-5 β -cholan-3 α ,24-diyl-3,24-sodium Disulfate (32). [α]₂₅^D +35.7 (c 0.11, CH₃OH). ¹H NMR (400 MHz, CD₃OD): δ 4.23 (1H, m), 3.96 (2H, t, *J* = 6.7 Hz), 3.48 (1H, m), 0.98 (3H, s), 0.97 (3H, d, *J* = 6.8 Hz), 0.71 (3H, s). HR ESIMS *m/z* 559.2015 [M – Na], C₂₄H₄₀NaO₉S₂ requires 559.2011.

7 β ,24-Dihydroxy-5 β -cholan-3 α -yl-3-sodium Sulfate (33). [α]₂₅^D +37.4 (c 0.08, CH₃OH). ¹H NMR (400 MHz, CD₃OD): δ 4.23 (1H, m), 3.50 (2H, m), 3.48 (1H, m), 0.97 (3H, s), 0.96 (3H, d, ovl), 0.71 (3H, s). HR ESIMS *m/z* 457.2627 [M – Na], C₂₄H₄₁O₆S requires 457.2624.

Ethyl 3 α ,7 β -Di(*tert*-butyldimethylsilyloxy)-25,26-bis-homo-5 β -chol-24-en-26-oate (34). Compound 34 (450 mg, 40% over two steps) was synthesized, starting from compound 29 (1.0 g, 1.6 mmol), by analogous procedures to those detailed above for compound 23. [α]₂₅^D +11.7 (c 0.58, CHCl₃). ¹H NMR (400 MHz, CDCl₃): δ 6.9 (1H, dt, *J* = 7.3, 15.5 Hz), 5.78 (1H, d, *J* = 15.5 Hz), 4.1 (2H, q, *J* = 7.3 Hz), 3.64 (1H, m), 3.50 (1H, br s), 1.26 (3H, t, *J* = 7.3 Hz), 0.91 (3H, d, ovl), 0.90 (3H, s), 0.86 (18H, s), 0.62 (3H, s), 0.04 (6H, s), 0.03 (6H, s). ¹³C NMR (100 MHz, CDCl₃): δ 167.0, 150.0, 120.9, 72.7, 72.5, 60.0, 55.5, 54.9, 43.9, 43.7, 42.8, 39.9, 38.8, 37.9, 37.8, 35.3 (2C), 35.1, 34.3, 34.1, 30.9 (2C), 30.8, 28.9, 27.3, 26.4 (3C), 25.9 (3C), 23.5, 21.2, 18.6, 14.3, 12.1, –2.8, –3.4, –4.6 (2C). HRMS-ESI *m/z* 675.5207 [M + H⁺], C₄₀H₇₅O₄Si₂ requires 675.5204.

3 α ,7 β -Di(*tert*-butyldimethylsilyloxy)-25,26-bis-homo-5 β -cholan-26-ol (35). A solution of compound 34 (400 mg, 0.6 mmol) in THF dry/MeOH dry (10 mL/10 mL, v/v) was hydrogenated in the presence of palladium, 5 wt %, on activated carbon (10 mg). The flask was evacuated and flushed first with argon and then with hydrogen. After 2 h, the reaction was complete. The catalyst was filtered through Celite, and the recovered filtrate was concentrated under vacuum to give the ethyl ester, which was used without any further purification.

Dry methanol (73 μ L, 1.8 mmol) and LiBH₄ (900 μ L, 2 M in THF, 1.8 mmol) were added to a solution of ethyl ester (400 mg, 0.6 mmol) in dry THF (15 mL) at 0 °C under argon, and the resulting mixture was stirred for 8 h at 0 °C. The mixture was quenched by addition of 1 M NaOH (1.2 mL) and then allowed to warm to room temperature. Ethyl acetate was added, and the separated aqueous phase was extracted with ethyl acetate (3 \times 30 mL). The combined organic phases were washed with water, dried (Na₂SO₄), and concentrated. Purification by silica gel (*n*-hexane/ethyl acetate 99:1) gave compound 35 as a colorless oil (334 mg, 88% over two steps). [α]₂₅^D +9.3 (c 0.4, CHCl₃). ¹H NMR (400 MHz, CDCl₃): δ 3.75 (2H, m), 3.65 (1H, m), 3.52 (1H, m), 0.92 (3H, s), 0.89 (3H, d, ovl), 0.89 (18H, s), 0.64 (3H,

s), 0.05 (6H, s), 0.04 (6H, s). ¹³C NMR (100 MHz, CDCl₃): δ 72.7, 72.5, 63.2, 55.5, 55.1, 43.9, 43.7, 42.8, 40.0, 38.8, 38.0, 37.8, 35.9 (2C), 35.6, 35.2, 34.1, 30.9 (2C), 30.8, 30.3, 29.7, 28.6, 27.3, 26.4 (3C), 25.9 (3C), 23.5, 21.2, 18.8, 12.1, –2.8, –3.3, –4.6 (2C). HRMS-ESI *m/z* 635.5257 [M + H⁺], C₃₈H₇₅O₃Si₂ requires 635.5255.

3 α ,7 β -Dihydroxy-25,26-bis-homo-5 β -cholan-26-yl-26-sodium Sulfate (36). Compound 36 (180 mg, 75% over two steps) was synthesized, starting from compound 35 (300 mg, 0.47 mmol), by procedures analogous to those detailed above for compound 30. [α]₂₅^D +14.7 (c 0.17, CH₃OH). Selected ¹H NMR (400 MHz, CD₃OD): δ 3.98 (2H, t, *J* = 6.5 Hz), 3.47 (2H, m), 0.96 (3H, s), 0.95 (3H, d, *J* = 6.0 Hz), 0.71 (3H, s). HR ESIMS *m/z* 485.2935 [M – Na], C₂₆H₄₅O₆S requires 485.2937.

25,26-Bis-homo-5 β -cholan-3 α ,7 β ,26-tryl-3,7,26-sodium Trisulfate (37) and 25,26-Bis-homo-7 β -hydroxy-5 β -cholan-3 α ,26-diyl-3,26-sodium disulfate (38). The triethylamine–sulfur trioxide complex (214 mg, 1.2 mmol) was added to a solution of compound 36 (60 mg, 0.12 mmol) in DMF dry (3 mL). The mixture was stirred at 95 °C for 5 h. Then the solution was concentrated under vacuum. The residue was poured over a RP18 column. The fraction eluted with H₂O/MeOH (7:3) gave a mixture that was further purified by HPLC, on a Nucleodur 100-5 C18 (5 μ m, 10 mm i.d. \times 250 mm) with MeOH/H₂O (35:65) as eluent (flow rate 3 mL/min), to give 37 and 38, 8 and 5 mg, respectively.

25,26-Bis-homo-5 β -cholan-3 α ,7 β ,26-tryl-3,7,26-sodium Trisulfate (37). [α]₂₅^D +3.34 (c 0.34, CH₃OH). Selected ¹H NMR (400 MHz, CD₃OD): δ 4.30 (1H, m), 4.23 (1H, m), 3.98 (2H, t, *J* = 6.6 Hz), 0.98 (3H, s), 0.95 (3H, d, *J* = 6.1 Hz), 0.70 (3H, s). HR ESIMS *m/z* 689.1715 [M – Na], C₂₆H₄₃Na₂O₁₂S₃ requires 689.1712.

25,26-Bis-homo-7 β -hydroxy-5 β -cholan-3 α ,26-diyl-3,26-sodium Disulfate (38). [α]₂₅^D +24.2 (c 0.11, CH₃OH). ¹H NMR (400 MHz, CD₃OD): δ 4.23 (1H, m), 3.96 (2H, t, *J* = 6.3 Hz), 3.48 (1H, m), 0.97 (3H, s), 0.95 (3H, d, *J* = 6.6 Hz), 0.70 (3H, s). HR ESIMS *m/z* 587.2329 [M – Na], C₂₆H₄₄NaO₉S₂ requires 587.2324.

Transactivation. HepG2 cells were cultured at 37 °C in minimum essential medium with Earl's salts containing 10% fetal bovine serum (FBS), 1% L-glutamine, and 1% penicillin/streptomycin. The transfection experiments were performed using Eugene HD (Promega) according to manufactured specifications. Cells were plated in a 24-well plate at 5 \times 10⁴ cells/well.

For FXR mediated transactivation, HepG2 cells were transfected with 75 ng of pSG5-FXR, 75 ng of pSG5-RXR, 100 ng of pCMV- β -galactosidase, and 250 ng of the reporter vector p(hsp27)-TK-LUC containing the FXR response element IRI cloned from the promoter of heat shock protein 27 (hsp27).

For GP-BAR1 mediated transactivation, HEK-293T cells were transfected with 200 ng of pGL4.29 (Promega), a reporter vector containing a cAMP response element (CRE) that drives the transcription of the luciferase reporter gene luc2P, with 100 ng of pCMVSPORT6-human GP-BAR1, and with 100 ng of pGL4.70 (Promega), a vector encoding the human Renilla gene.

In control experiments HEK-293T cells were transfected only with vectors pGL4.29 and pGL4.70 to exclude any possibility that compounds could activate the CRE in a GP-BAR1 independent manner. At 24 h post-transfection, cells were stimulated 18 h with CDCA (3) at 10 μ M, 1 (1 and 10 μ M), and compounds 2, 3, 13, 18–21, 26, 27, 30–33, and 36–38, 10 μ M; in another experimental setting, cells were primed with the combination of CDCA (3) at 10 μ M and compounds 13, 18, 20, 21, 27, 30–33, and 36–38 (50 μ M). After treatments, cells were lysed in 100 μ L of lysis buffer (25 mM Tris-phosphate, pH 7.8; 2 mM DTT; 10% glycerol; 1% Triton X-100), and 20 μ L of cellular lysate was assayed for luciferase activity using the luciferase assay system (Promega). Luminescence was measured using Glomax 20/20 luminometer (Promega). For FXR mediated transactivation, luciferase activities were normalized for transfection efficiencies by dividing the luciferase relative light units by β -galactosidase activity expressed from cells co-transfected with pCMV β gal. For GP-BAR1 mediated transactivation, luciferase activities were normalized with Renilla activities.

To realize dose–response curves for compound **19**, cells were transfected as described previously and then treated with increasing concentrations of **19** (0.01, 0.1, 1, and 10 μ M). Luciferase activities were assayed and normalized as described above in order to calculate EC₅₀.

GLUTAg cells were kindly donated by Dr. D. J. Drucker, Banting and Best Diabetes Centre, University of Toronto, Toronto General Hospital, 200 Elizabeth Street MBRW-4R402, Toronto, Canada M5G 2C4.

FXR^{-/-} mice were originally donated by Dr. F. Gonzalez, Laboratory of Metabolism, Center for Cancer Research, National Cancer Institute, National Institutes of Health, Bethesda, Maryland 20892, U.S., as previously reported.⁵⁵

Cells were plated in a 24-well plate at 5×10^4 cells/well, and the transfection experiments were performed using Fugene HD (Promega) according to manufactured specifications.

Real-Time PCR. PCR was performed using Primers, and experimental conditions were as described previously.⁵²

cAMP and GLP-1 Measurement. cAMP and GLP-1 release in GLUTAg cells were measured as described previously.²⁰

Homology Modeling. The crystal structure of human adenosine A_{2A} receptor (PDB code 2ydo)⁴⁴ was used as template to build the homology model of human GP-BAR1. First a multiple alignment of the sequence of different GPCRs (adenosine receptors, histamine H2 receptor, sphingosine 1-phosphate receptors, cannabinoid receptors, muscarinic acetylcholine receptors, dopamine receptor, rhodopsin, etc.) was performed using ClustalW^{56,57} to identify the most conserved regions along the GP-BAR1 sequence (Swissprot ID code q8td6). Then we chose as template the agonist conformation of the adenosine A_{2A} receptor that shows one of the highest sequence identity and similarity values, 20% and 55%, respectively (Figure S2). The alignment between the model (GP-BAR1) and the template (A_(2A)R-GL31) primary sequence was refined considering highly conserved amino acid residues among GPCRs. In particular, in the extracellular region, where the ligand binding site is located, the presence of the disulfide bond between Cys85 and Cys155 of the extracellular loop II (EL2) and the transmembrane helix III (TM3), respectively, was considered. Finally, using Modeller, version 9.11,⁵⁸ we built the tridimensional structure of the GP-BAR1 receptor.

The homology model of GP-BAR1 was embedded in a POPC phospholipids bilayer to mimic the physiological environment and submitted first to minimization and then to a 100 ns long MD simulation to check its stability (see section on molecular dynamics methods). A geometric validation of the tridimensional structure of the receptor used in the docking calculations was carried out using the MolProbity server (<http://molprobity.biochem.duke.edu>). The model shows ~94% of all residues in favored conformational regions and 100% in allowed ones according to the Ramachandran analysis and 0% of backbone bonds and angles with bad values (Figure S4).

Molecular Docking. Molecular docking calculations in the rFXR-LBD X-ray structure (PDB code 1osv)⁵¹ and in the three-dimensional model of hGP-BAR1 were carried out using the AutoDock4.2 software package.⁴⁵ Ligand tridimensional structures were generated with the Maestro build panel.⁵⁹ For each ligand, an extensive ring conformational sampling was performed with the OPLS-AA force field⁶⁰ and a 2.0 Å rmsd cutoff using MacroModel (version 9.9)⁶¹ as implemented in Maestro 9.3.⁵⁹ All conformers were then refined using LigPrep⁶² as implemented in Maestro 9.3.⁵⁹ Protonation states at pH 7.0 were assigned using Epik.⁶³ Protein structure was prepared through the Protein Preparation Wizard through the graphical user interface of Maestro 9.3.⁵⁹ Water molecules were removed, and hydrogen atoms were added and minimized using the OPLS-2005 force field.⁶⁰ Ligands and receptor structures were converted to AD4 format files using ADT, and the Gasteiger–Marsili partial charges were then assigned. Grid points of $70 \times 70 \times 70$ for FXR and of $65 \times 80 \times 55$ for GP-BAR1 with a 0.375 Å spacing were calculated around the binding cavity using AutoGrid4.2. Thus, 100 separate docking calculations were performed for each run. Each docking run consisted of 10 million energy evaluations using the Lamarckian genetic algorithm local search (GALS) method. Otherwise default docking parameters were applied.

Docking conformations were clustered on the basis of their rmsd (tolerance = 2.0 Å) and were ranked based on the AutoDock scoring function.⁴⁵

Molecular Dynamics. The same computational protocol was used to set up both the apo GP-BAR1-membrane and the GP-BAR1/1-membrane complexes. A $94 \text{ \AA} \times 94 \text{ \AA}$ (in *x* and *y* axes) pre-equilibrated POPC phospholipid bilayer was initially generated using the membrane-builder tool of CHARMM-GUI.org (<http://www.charmm-gui.org>). In order to place the receptor into the bilayer, a hole was generated, and all lipids in close contact (<1 Å distance from any protein atoms) were deleted. Each complex was solvated and neutralized using the solvation and autoionize modules of VMD 1.9.1.⁶⁴ The TIP3 water model⁶⁵ was used to treat the solvent. The *ff99SBildn*,^{66,67} *gaff*,⁶⁸ and *lipid11*⁶⁹ Amber force fields were used to parametrize the protein, the ligand, and the lipids, respectively. All the simulations were performed with the NAMD 2.8 MD code.⁷⁰ A 10 Å cutoff (switched at 8.0 Å) was used for atom–pair interactions. The long-range electrostatic interactions were computed by means of the particle mesh Ewald (PME) method⁷¹ using a 1.0 Å grid spacing in periodic boundary conditions. The SHAKE algorithm was applied to constrain bonds involving hydrogen atoms, and thus an integration 2 fs time step interval could be used. Amber charges were applied to the proteins and water molecules, whereas the ligand charges were computed using the restrained electrostatic potential (RESP) fitting procedure.⁷² The ESP was first calculated by means of the Gaussian 03 package⁷³ using a 6-31G* basis set at Hartree–Fock level of theory, and then the RESP charges were obtained by a two-stage fitting procedure using Antechamber.⁷⁴ The system was equilibrated in the NPT ensemble using a target temperature and pressure of 300 K and 1 atm, respectively. Harmonic constraints were applied to the protein and the ligand, which were gradually released along the equilibration process.

Production runs were performed in NPT conditions at 1 atm and 300 K.

All the residue labels were taken from crystal structure of rFXR-LBD with PDB code 1osv and the wild-type amino acidic sequence of human GP-BAR1.

All figures were rendered using PyMOL (<http://www.pymol.org>). The tridimensional model of GP-BAR1 is available upon request.

■ ASSOCIATED CONTENT

📄 Supporting Information

Tabulated NMR data for **1**; activation of cAMP responsive gene in absence of GP-BAR1 (Figure S1); alignment GP-BAR1/template A(2A)R-GL31 (Figure S2); protein backbone rmsd of GP-BAR1 model (Figure S3); Ramachandran plot of the GP-BAR1 structure (Figure S4); binding modes of 6-ECDCA in GP-BAR1 and FXR (Figure S5); tridimensional movie showing the stability of the binding mode of **1** to GP-BAR1; NMR proton spectra for all tested compounds. This material is available free of charge via the Internet at <http://pubs.acs.org>.

■ AUTHOR INFORMATION

Corresponding Authors

*A.Z.: phone, +39 081 678525; fax, +39 081 678552; e-mail, angela.zampella@unina.it.

*V.L.: phone, +39 081 678 641; e-mail, vittoriolimongelli@gmail.com.

Author Contributions

||C.D., F.S.D.L., and V.S. contributed equally to this work.

Notes

The authors declare no competing financial interest.

■ ACKNOWLEDGMENTS

This work was supported by grants from MAREX-Exploring Marine Resources for Bioactive Compounds: From Discovery

to Sustainable Production and Industrial Applications (Call FP7-KBBE-2009-3, Project No. 245137), MIUR-PRIN 2010/2011 (Grant E61J12000210001), Swiss National Supercomputing Centre (CSCS, Project s386), and from PSC Partners foundation.

■ ABBREVIATIONS USED

AD4.2, AutoDock4.2; BA, bile acid; BSEP, bile salt export pump; CAR, constitutive androstane receptor; CDCA, chenodeoxycholic acid; 6-ECDCA, 6-ethylchenodeoxycholic acid; FXR, farnesoid X receptor; GLP-1, glucagon-like peptide 1; GPCR, G-protein-coupled receptor; GP-BAR-1, G-protein-coupled bile acid receptor 1; HepG2, human hepatoma cell line; LBD, ligand binding domain; LCA, lithocholic acid; LXR, liver X receptor; M-BAR/TGR5, membrane-type bile acid receptor/Takeda G-protein-coupled receptor; MD, molecular dynamics; NR, nuclear receptor; OST α , organic solute transporter α ; PXR, pregnane X receptor; RXR, retinoid X receptor; RT-PCR, real-time polymerase chain reaction; SHP, small heterodimer partner; TLCA, tauroolithocholic acid; UDCA, ursodeoxycholic acid; VDR, vitamin D receptor; HEK-293T, human embryonic kidney 293T

■ REFERENCES

(1) de Aguiar Vallim, T. Q.; Tarling, E. J.; Edwards, P. A. Pleiotropic roles of bile acids in metabolism. *Cell Metab.* **2013**, *17*, 657–669.

(2) Makishima, M.; Okamoto, A. Y.; Repa, J. J.; Tu, H.; Learned, R. M.; Luk, A.; Hull, M. V.; Lustig, K. D.; Mangelsdorf, D. J.; Shan, B. Identification of a nuclear receptor for bile acids. *Science* **1999**, *284*, 1362–1365.

(3) Parks, D. J.; Blanchard, S. G.; Bledsoe, R. K.; Chandra, G.; Consler, T. G.; Kliewer, S. A.; Stimmel, J. B.; Willson, T. M.; Zavacki, A. M.; Moore, D. D.; Lehmann, J. M. Bile acids: natural ligands for an orphan nuclear receptor. *Science* **1999**, *284*, 1365–1368.

(4) Zhang, Y.; Lee, F. Y.; Barrera, G.; Lee, H.; Vales, C.; Gonzalez, F. J.; Willson, T. M.; Edwards, P. A. Activation of the nuclear receptor FXR improves hyperglycemia and hyperlipidemia in diabetic mice. *Proc. Natl. Acad. Sci. U.S.A.* **2006**, *103*, 1006–1011.

(5) Renga, B.; Mencarelli, A.; D'Amore, C.; Cipriani, S.; Baldelli, F.; Zampella, A.; Distrutti, E.; Fiorucci, S. Glucocorticoid receptor mediates the gluconeogenic activity of the farnesoid X receptor in the fasting condition. *FASEB J.* **2012**, *26*, 3021–3031.

(6) Wang, Y. D.; Chen, W. D.; Wang, M.; Yu, D.; Forman, B. M.; Huang, W. Farnesoid X receptor antagonizes nuclear factor κ B in hepatic inflammatory response. *Hepatology* **2008**, *48*, 1632–1643.

(7) Fiorucci, S.; Rizzo, G.; Antonelli, E.; Renga, B.; Mencarelli, A.; Riccardi, L.; Orlandi, S.; Pruzanski, M.; Morelli, A.; Pellicciari, R. A farnesoid X receptor-small heterodimer partner regulatory cascade modulates tissue metalloproteinase inhibitor-1 and matrix metalloproteinase expression in hepatic stellate cells and promotes resolution of liver fibrosis. *J. Pharmacol. Exp. Ther.* **2005**, *314*, 584–595.

(8) Baptissart, M.; Vega, A.; Maqdasy, S.; Caira, F.; Baron, S.; Lobaccaro, J. M.; Volle, D. H. Bile acids: from digestion to cancers. *Biochimie* **2013**, *95*, 504–517.

(9) Staudinger, J. L.; Goodwin, B.; Jones, S. A.; Hawkins-Brown, D.; MacKenzie, K. I.; LaTour, A.; Liu, Y.; Klaassen, C. D.; Brown, K. K.; Reinhard, J.; Willson, T. M.; Koller, B. H.; Kliewer, S. A. The nuclear receptor PXR is a lithocholic acid sensor that protects against liver toxicity. *Proc. Natl. Acad. Sci. U.S.A.* **2001**, *98*, 3369–3374.

(10) Makishima, M.; Lu, T. T.; Xie, W.; Whitfield, G. K.; Domoto, H.; Evans, R. M.; Haussler, M. R.; Mangelsdorf, D. J. Vitamin D receptor as an intestinal bile acid sensor. *Science* **2002**, *296*, 1313–1316.

(11) Kohle, C.; Bock, K. W. Coordinate regulation of human drug-metabolizing enzymes, and conjugate transporters by the Ah receptor,

pregnane X receptor and constitutive androstane receptor. *Biochem. Pharmacol.* **2009**, *77*, 689–699.

(12) Takeda, S.; Kadowaki, S.; Haga, T.; Takaesu, H.; Mitaku, S. Identification of G protein-coupled receptor genes from the human genome sequence. *FEBS Lett.* **2002**, *520*, 97–101.

(13) Maruyama, T.; Miyamoto, Y.; Nakamura, T.; Tamai, Y.; Okada, H.; Sugiyama, E.; Nakamura, T.; Itadani, H.; Tanaka, K. Identification of membrane type receptor for bile acids (M-BAR). *Biochem. Biophys. Res. Commun.* **2002**, *298*, 714–719.

(14) Kawamata, Y.; Fujii, R.; Hosoya, M.; Harada, M.; Yoshida, H.; Miwa, M.; Fukusumi, S.; Habata, Y.; Itoh, T.; Shintani, Y.; Hinuma, S.; Fujisawa, Y.; Fujino, M. A G protein-coupled receptor responsive to bile acids. *J. Biol. Chem.* **2003**, *278*, 9435–9440.

(15) Watanabe, M.; Houten, S. M.; Matak, C.; Christoffolete, M. A.; Kim, B. W.; Sato, H.; Messaddeq, N.; Harney, J. W.; Ezaki, O.; Kodama, T.; Schoonjans, K.; Bianco, A. C.; Auwerx, J. Bile acids induce energy expenditure by promoting intracellular thyroid hormone activation. *Nature* **2006**, *439*, 484–489.

(16) Thomas, C.; Gioiello, A.; Noriega, L.; Strehle, A.; Oury, J.; Rizzo, G.; Macchiarulo, A.; Yamamoto, H.; Matak, C.; Pruzanski, M.; Pellicciari, R.; Auwerx, J.; Schoonjans, K. TGR5-mediated bile acid sensing controls glucose homeostasis. *Cell Metab.* **2009**, *10*, 167–177.

(17) Pellicciari, R.; Sato, H.; Gioiello, A.; Costantino, G.; Macchiarulo, A.; Sadeghpour, B. M.; Giorgi, G.; Schoonjans, K.; Auwerx, J. Nongenomic actions of bile acids. Synthesis and preliminary characterization of 23- and 6,23-alkyl-substituted bile acid derivatives as selective modulators for the G-protein coupled receptor TGR5. *J. Med. Chem.* **2007**, *50*, 4265–4268.

(18) Wang, Y. D.; Chen, W. D.; Yu, D.; Forman, B. M.; Huang, W. The G-protein-coupled bile acid receptor, Gpbar1 (TGR5), negatively regulates hepatic inflammatory response through antagonizing nuclear factor kappa light-chain enhancer of activated B cells (NF- κ B) in mice. *Hepatology* **2011**, *54*, 1421–1432.

(19) Cipriani, S.; Mencarelli, A.; Chini, M. G.; Distrutti, E.; Renga, B.; Bifulco, G.; Baldelli, F.; Donini, A.; Fiorucci, S. The bile acid receptor GPBAR-1 (TGR5) modulates integrity of intestinal barrier and immune response to experimental colitis. *PLoS One* **2011**, *6*, e25637.

(20) Cipriani, S.; Mencarelli, A.; Bruno, A.; Renga, B.; Distrutti, E.; Santucci, L.; Baldelli, F.; Fiorucci, S. Activation of the bile acid receptor GPBAR1 protects against gastrointestinal injury caused by non-steroidal anti-inflammatory drugs and aspirin in mice. *Br. J. Pharmacol.* **2013**, *168*, 225–237.

(21) Fiorucci, S.; Mencarelli, A.; Palladino, G.; Cipriani, S. Bile-acid-activated receptors: targeting TGR5 and farnesoid-X-receptor in lipid and glucose disorders. *Trends Pharmacol. Sci.* **2009**, *30*, 570–580.

(22) Fiorucci, S.; Cipriani, S.; Baldelli, F.; Mencarelli, A. Bile acid-activated receptors in the treatment of dyslipidemia and related disorders. *Prog. Lipid Res.* **2010**, *49*, 171–185.

(23) Cipriani, S.; Mencarelli, A.; Palladino, G.; Fiorucci, S. FXR activation reverses insulin resistance and lipid abnormalities and protects against liver steatosis in Zucker (fa/fa) obese rats. *J. Lipid Res.* **2010**, *51*, 771–784.

(24) Baghdasaryan, A.; Claudel, T.; Gumhold, J.; Silbert, D.; Adorini, L.; Roda, A.; Vecchiotti, S.; Gonzalez, F. J.; Schoonjans, K.; Strazzabosco, M.; Fickert, P.; Trauner, M. Dual farnesoid X receptor/TGR5 agonist INT-767 reduces liver injury in the Mdr2 $^{-/-}$ (Abcb4 $^{-/-}$) mouse cholangiopathy model by promoting biliary HCO $_{3}^{-}$ output. *Hepatology* **2011**, *54*, 1303–1312.

(25) Rizzo, G.; Passeri, D.; De Franco, F.; Ciaccioli, G.; Donadio, L.; Rizzo, G.; Orlandi, S.; Sadeghpour, B.; Wang, X. X.; Jiang, T.; Levi, M.; Pruzanski, M.; Adorini, L. Functional characterization of the semisynthetic bile acid derivative INT-767, a dual farnesoid X receptor and TGR5 agonist. *Mol. Pharmacol.* **2010**, *78*, 617–630.

(26) Pellicciari, R.; Fiorucci, S.; Pruzanski, M. Preparation of Bile Acid Derivatives as FXR Ligands for the Prevention or Treatment of FXR-Mediated Diseases or Conditions. PCT Int. WO 2008002573 A2 20080103, 2008.

- (27) Sepe, V.; Ummarino, R.; D'Auria, M. V.; Chini, M. G.; Bifulco, G.; Renga, B.; D'Amore, C.; Debitus, C.; Fiorucci, S.; Zampella, A. Conicasterol E, a small heterodimer partner sparing farnesoid X receptor modulator endowed with a pregnane X receptor agonistic activity, from the marine sponge *Theonella swinhoei*. *J. Med. Chem.* **2012**, *55*, 84–93.
- (28) Gioiello, A.; Macchiarulo, A.; Carotti, A.; Filippini, P.; Costantino, G.; Rizzo, G.; Adorini, L.; Pellicciari, R. Extending SAR of bile acids as FXR ligands: discovery of 23-N-(carbocinnamyloxy)-3 α ,7 α -dihydroxy-6 α -ethyl-24-nor-5 β -cholan-23-amine. *Bioorg. Med. Chem.* **2011**, *19*, 2650–2658.
- (29) Sepe, V.; Ummarino, R.; D'Auria, M. V.; Renga, B.; Fiorucci, S.; Zampella, A. The first total synthesis of solomonsterol B, a marine pregnane X receptor agonist. *Eur. J. Org. Chem.* **2012**, 5187–5194.
- (30) Tserng, K. Y.; Klein, P. D. Formylated bile acids: improved synthesis, properties, and partial deformylation. *Steroids* **1977**, *29*, 635–648.
- (31) Schteingart, C. D.; Hofmann, A. F. Synthesis of 24-nor-5 β -cholan-23-oic acid derivatives: a convenient and efficient one-carbon degradation of the side chain of natural bile acids. *J. Lipid Res.* **1988**, *29*, 1387–1395.
- (32) Mancuso, A. J.; Swern, D. Activated dimethyl sulfoxide: useful reagents for synthesis. *Synthesis* **1981**, *3*, 165–185.
- (33) Nagoka, H.; Kishi, Y. Further synthetic studies on rifamycin S. *Tetrahedron* **1981**, *37*, 3873–3888.
- (34) Fujino, T.; Une, M.; Imanaka, T.; Inoue, K.; Nishimaki-Mogami, T. Structure–activity relationship of bile acids and bile acid analogs in regard to FXR activation. *J. Lipid Res.* **2004**, *45*, 132–138.
- (35) Pellicciari, R.; Fiorucci, S.; Camaioni, E.; Clerici, C.; Costantino, G.; Maloney, P. R.; Morelli, A.; Parks, D. J.; Willson, T. M. 6- α -Ethylchenodeoxycholic acid (6-ECDCA), a potent and selective FXR agonist endowed with anticholestatic activity. *J. Med. Chem.* **2002**, *45*, 3569–3572.
- (36) Fiorucci, S.; Cipriani, S.; Mencarelli, A.; Baldelli, F.; Bifulco, G.; Zampella, A. Farnesoid X receptor agonist for the treatment of liver and metabolic disorders: focus on 6-ethyl-CDCA. *Mini-Rev. Med. Chem.* **2011**, *11*, 753–762.
- (37) Parker, H. E.; Wallis, K.; le Roux, C. W.; Wong, K. Y.; Reimann, F.; Gribble, F. M. Molecular mechanisms underlying bile acid-stimulated glucagon-like peptide-1 secretion. *Br. J. Pharmacol.* **2012**, *165*, 414–423.
- (38) Petersen, A. B.; Christensen, M. Clinical potential of lixisenatide once daily treatment for type 2 diabetes mellitus. *Diabetes, Metab. Syndr. Obes.* **2013**, *6*, 217–231.
- (39) Nauck, M. A.; Baranov, O.; Ritzel, R. A.; Meier, J. J. Do current incretin mimetics exploit the full therapeutic potential inherent in GLP-1 receptor stimulation? *Diabetologia* **2013**, *56*, 1878–1883.
- (40) Scheen, A. J. Cardiovascular effects of dipeptidyl peptidase-4 inhibitors: from risk factors to clinical outcomes. *Postgrad. Med.* **2013**, *125*, 7–20.
- (41) Cohen, D. Reports of pancreatitis are 20–30 times more likely with GLP-1 drugs, analysis finds. *Br. Med. J.* **2013**, *346*, f2607.
- (42) Butler, A. E.; Campbell-Thompson, M.; Gurlo, T.; Dawson, D. W.; Atkinson, M.; Butler, P. C. Marked expansion of exocrine and endocrine pancreas with incretin therapy in humans with increased exocrine pancreas dysplasia and the potential for glucagon-producing neuroendocrine tumors. *Diabetes* **2013**, *62*, 2595–2604.
- (43) Fiorucci, S.; Distrutti, E.; Bifulco, G.; D'Auria, M. V.; Zampella, A. Marine sponge steroids as nuclear receptor ligands. *Trends Pharmacol. Sci.* **2012**, *33*, 591–601.
- (44) Lebon, G.; Warne, T.; Edwards, P. C.; Bennett, K.; Langmead, C. J.; Leslie, A. G.; Tate, C. G. Agonist-bound adenosine A_{2A} receptor structures reveal common features of GPCR activation. *Nature* **2011**, *474*, 521–525.
- (45) Huey, R.; Morris, G. M.; Olson, A. J.; Goodsell, D. S. A semiempirical free energy force field with charge-based desolvation. *J. Comput. Chem.* **2007**, *28*, 1145–1152.
- (46) Tiwari, A.; Maiti, P. TGR5: an emerging bile acid G-protein-coupled receptor target for the potential treatment of metabolic disorders. *Drug Discovery Today* **2009**, *14*, 523–530.
- (47) Grazioso, G.; Limongelli, V.; Branduardi, D.; Novellino, E.; De Micheli, C.; Cavalli, A.; Parrinello, M. Investigating the mechanism of substrate uptake and release in the glutamate transporter homologue GltPh through metadynamics simulations. *J. Am. Chem. Soc.* **2012**, *134*, 453–463.
- (48) Limongelli, V.; Bonomi, M.; Parrinello, M. Funnel metadynamics as accurate binding free-energy method. *Proc. Natl. Acad. Sci. U.S.A.* **2013**, *110*, 6358–6363.
- (49) Limongelli, V.; Marinelli, L.; Cosconati, S.; La Motta, C.; Sartini, S.; Mugnaini, L.; Da Settimo, F.; Novellino, E.; Parrinello, M. Sampling protein motion and solvent effect during ligand binding. *Proc. Natl. Acad. Sci. U.S.A.* **2012**, *109*, 1467–1472.
- (50) Macchiarulo, A.; Gioiello, A.; Thomas, C.; Pols, T. W. H.; Nuti, R.; Ferrari, C.; Giacche, N.; De Franco, F.; Pruzanski, M.; Auwerx, J.; Schoonjans, K.; Pellicciari, R. Probing the binding site of bile acids in TGR5. *ACS Med. Chem. Lett.* **2013**, *4*, 1158–1162.
- (51) Mi, L. Z.; Devarakonda, S.; Harp, J. M.; Han, Q.; Pellicciari, R.; Willson, T. M.; Khorasanizadeh, S.; Rastinejad, F. Structural basis for bile acid binding and activation of the nuclear receptor FXR. *Mol. Cell* **2003**, *11*, 1093–1100.
- (52) Di Leva, F. S.; Festa, C.; D'Amore, C.; De Marino, S.; Renga, B.; D'Auria, M. V.; Novellino, E.; Limongelli, V.; Zampella, A.; Fiorucci, S. Binding mechanism of the farnesoid X receptor marine antagonist suvanine reveals a strategy to forestall drug modulation on nuclear receptors. Design, synthesis, and biological evaluation of novel ligands. *J. Med. Chem.* **2013**, *56*, 4701–4717.
- (53) Brubaker, P. L.; Schloos, J.; Drucker, D. J. Regulation of glucagon-like peptide-1 synthesis and secretion in the GLUTag enteroendocrine cell line. *Endocrinology* **1998**, *139*, 4108–4114.
- (54) Fiorucci, S.; Baldelli, F. Farnesoid X receptor agonists in biliary tract disease. *Curr. Opin. Gastroenterol.* **2009**, *25*, 252–259.
- (55) Mencarelli, A.; Renga, B.; Migliorati, M.; Cipriani, S.; Distrutti, E.; Santucci, L.; Fiorucci, S. The bile acid sensor farnesoid X receptor is a modulator of liver immunity in a rodent model of acute hepatitis. *J. Immunol.* **2009**, *183*, 6657–6666.
- (56) Chenna, R.; Sugawara, H.; Koike, T.; Lopez, R.; Gibson, T. J.; Higgins, D. G.; Thompson, J. D. Multiple sequence alignment with the Clustal series of programs. *Nucleic Acids Res.* **2003**, *31*, 3497–3500.
- (57) Larkin, M. A.; Blackshields, G.; Brown, N. P.; Chenna, R.; McGettigan, P. A.; McWilliam, H.; Valentin, F.; Wallace, I. M.; Wilm, A.; Lopez, R.; Thompson, J. D.; Gibson, T. J.; Higgins, D. G. ClustalW and ClustalX version 2. *Bioinformatics* **2007**, *23*, 2947–2948.
- (58) Sali, A.; Blundell, T. L. Comparative protein modelling by satisfaction of spatial restraints. *J. Mol. Biol.* **1993**, *234*, 779–815.
- (59) *Maestro*, version 9.3; Schrödinger, LLC: New York, NY, 2012.
- (60) Jorgensen, W. L.; Maxwell, D. S.; Tirado-Rives, J. Development and testing of the OPLS all-atom force field on conformational energetics and properties of organic liquids. *J. Am. Chem. Soc.* **1996**, *118*, 11225–11236.
- (61) *MacroModel*, version 9.9; Schrödinger, LLC: New York, NY, 2012.
- (62) *LigPrep*, version 2.5; Schrödinger, LLC: New York, NY, 2012.
- (63) *Epik*, version 2.3; Schrödinger, LLC: New York, NY, 2012.
- (64) Humphrey, W.; Dalke, A.; Schulten, K. VMD: visual molecular dynamics. *J. Mol. Graphics* **1996**, *14*, 33–38.
- (65) Jorgensen, W. L.; Chandrasekhar, J.; Madura, J. D.; Impey, R. W.; Klein, M. L. Comparison of simple potential functions for simulating liquid water. *J. Chem. Phys.* **1983**, *79*, 926–935.
- (66) Cornell, W. D.; Cieplak, P.; Bayly, C. I.; Gould, I. R.; Merz, K. M.; Ferguson, D. M.; Spellmeyer, D. C.; Fox, T.; Caldwell, J. W.; Kollman, P. A. A second generation force field for the simulation of proteins, nucleic acids, and organic molecules. *J. Am. Chem. Soc.* **1995**, *117*, 5179–5197.
- (67) Lindorff-Larsen, K.; Piana, S.; Palmo, K.; Maragakis, P.; Klepeis, J. L.; Dror, R. O.; Shaw, D. E. Improved side-chain torsion potentials

for the Amber ff99SB protein force field. *Proteins* **2010**, *78*, 1950–1958.

(68) Wang, J.; Wolf, R. M.; Caldwell, J. W.; Kollman, P. A.; Case, D. A. Development and testing of a general amber force field. *J. Comput. Chem.* **2004**, *25*, 1157–1174.

(69) Skjevik, Å. A.; Madej, B. D.; Walker, R. C.; Teigen, K. LIPID11: a modular framework for lipid simulations using Amber. *J. Phys. Chem. B* **2012**, *116*, 11124–11136.

(70) Phillips, J. C.; Braun, R.; Wang, W.; Gumbart, J.; Tajkhorshid, E.; Villa, E.; Chipot, C.; Skeel, R. D.; Kalé, L.; Schulten, K. Scalable molecular dynamics with NAMD. *J. Comput. Chem.* **2005**, *26*, 1781–1802.

(71) Darden, T.; York, D.; Pedersen, L. Particle mesh Ewald: an $N \log(N)$ method for Ewald sums in large systems. *J. Chem. Phys.* **1993**, *98*, 10089–10092.

(72) Bayly, C. I.; Cieplak, P.; Cornell, W. D.; Kollman, P. A. A well-behaved electrostatic potential based method using charge restraints for determining atom-centered charges: the RESP model. *J. Phys. Chem.* **1993**, *97*, 10269–10280.

(73) Frisch, M. J.; Trucks, G. W.; Schlegel, H. B.; Scuseria, G. E.; Robb, M. A.; Cheeseman, J. R.; Montgomery, J. A., Jr.; Vreven, T.; Kudin, K. N.; Burant, J. C.; Millam, J. M.; Iyengar, S. S.; Tomasi, J.; Barone, V.; Mennucci, B.; Cossi, M.; Scalmani, G.; Rega, N.; Petersson, G. A.; Nakatsuji, H.; Hada, M.; Ehara, M.; Toyota, K.; Fukuda, R.; Hasegawa, J.; Ishida, M.; Nakajima, T.; Honda, Y.; Kitao, O.; Nakai, H.; Klene, M.; Li, X.; Knox, J. E.; Hratchian, H. P.; Cross, J. B.; Bakken, V.; Adamo, C.; Jaramillo, J.; Gomperts, R.; Stratmann, R. E.; Yazyev, O.; Austin, A. J.; Cammi, R.; Pomelli, C.; Ochterski, J. W.; Ayala, P. Y.; Morokuma, K.; Voth, G. A.; Salvador, P.; Dannenberg, J. J.; Zakrzewski, V. G.; Dapprich, S.; Daniels, A. D.; Strain, M. C.; Farkas, O.; Malick, D. K.; Rabuck, A. D.; Raghavachari, K.; Foresman, J. B.; Ortiz, J. V.; Cui, Q.; Baboul, A. G.; Clifford, S.; Cioslowski, J.; Stefanov, B. B.; Liu, G.; Liashenko, A.; Piskorz, P.; Komaromi, I.; Martin, R. L.; Fox, D. J.; Keith, T.; Al-Laham, M. A.; Peng, C. Y.; Nanayakkara, A.; Challacombe, M.; Gill, P. M. W.; Johnson, B.; Chen, W.; Wong, M. W.; Gonzalez, C.; Pople, J. A. *Gaussian 03*; Gaussian, Inc.: Wallingford, CT, 2004.

(74) Wang, J.; Wang, W.; Kollman, P. A.; Case, D. A. Automatic atom type and bond type perception in molecular mechanics. *J. Mol. Graphics Modell.* **2006**, *25*, 247–260.